A REAL TIME HF BEACON MONITORING STATION FOR SOUTH AFRICA

A thesis submitted in partial fulfilment of the requirements for the degree of

MASTER OF SCIENCE

of

Rhodes University

by

Courage Mudzingwa

June 2009

Abstract

High frequency, HF (3 - 30 MHz), radio communications are greatly affected by ionospheric conditions. Both civilian and military users need reliable, real time propagation information to show at any time the feasibility of communicating to any part of the world on a particular frequency band. For this thesis, an automated receiving/monitoring station for the Northern California DX Foundation (NCDXF)/ International Amateur Radio Union (IARU) International Beacon Project was setup at the Hermanus Magnetic Observatory, HMO (34.42°S, 19.22°E) to monitor international beacons on 20 m, 17 m, 15 m, 12 m and 10 m bands. The beacons form a world wide multiband network. The task of monitoring the beacons was broken down into two steps. Initially the single band station, at 14.10 MHz, was installed and later it was upgraded to a multiband station capable of automatically monitoring all the five HF bands. The single band station setup involved the construction and installation of the half-wave dipole antenna, construction and installation of an HF choke balun; and the choice of Faros 1.3 as the appropriate monitoring software. The multiband monitoring station set-up involved the installation of an MFJ-1778 G5RV multiband antenna, construction and installation of a Communication Interface - V (CI-V) level converter and configuring the Faros 1.3 software to monitor the beacons on all five HF bands. Then a web page was created on the HMO space weather website (http://spaceweather.hmo.ac.za). Here, the real-time signal to noise ratio (SNR) and short path (SP)/long path (LP) plots are uploaded every 3 minutes, showing real time HF propagation conditions on the five HF bands. Historical propagation data are archived for later analysis. A preliminary data analysis was done to confirm the operation of the monitoring station. The archived data were analysed and compared to ICEPAC (Ionospheric Communications Enhanced Profile Analysis and Circuit) predictions. Results show that the real-time signal plots as well as the archive of historical signal plots, convey information on propagation conditions to users in terms that are easy to interpret and understand.

Acknowledgements

I would like to thank my supervisors Dr. L.A. McKinnell and Mr. Lindsay Magnus for providing all the necessary insights and guidance throughout the project to make it a success. I also extend my gratitude to my parents and family for their unwavering support during this period of study away from home.

I would like to express my appreciation to the National Astrophysics and Space Science Programme (NASSP), South Africa for funding my studies.

Contents

List of figures

List of tables

Chapter 1

Introduction

1.1 Background

The material in this thesis aims at presenting the work that was carried out to provide a high frequency (HF) automatic monitoring station in South Africa as a means to provide useful real-time propagation information to amateur and commercial radio operators, as well as the defence community, through the continuous monitoring of the international HF beacons. The monitoring station also allows us to gather and archive propagation path data for the purpose of validating prediction software. The beacons monitored in this project are maintained by the Northern California DX Foundation (NCDXF)/International Amateur Radio Union (IARU) International Beacon Project.

1.1.1 Long-distance HF propagation

The ionosphere is a region of very low density atmosphere which begins at an altitude of about 50 km and extends up to beyond 1000 km. HF radio propagation depends upon the ability of the ionosphere to return the radio signals back to Earth. Radio communications in the HF band (3 - 30 MHz) relies on sky wave propagation over long distances (Laster, 2000). A sky wave is a radio wave refracted back to the Earth's surface by the ionosphere whereas a ground wave is a radio wave that travels along the surface of the Earth. In the HF band, propagation of a sky wave supplements the ground wave. Sky wave propagation between two locations on the Earth's surface takes place by combinations of reflections from the ionospheric layers and the Earth's surface, as shown in Figure 1.1.

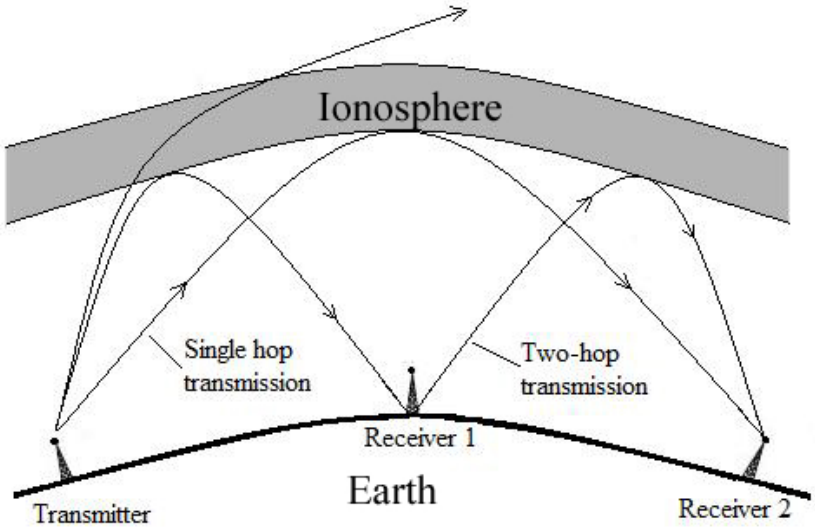

Figure 1.1: HF propagation through the ionosphere (*after* Carr, 2001b).

Figure 1.1 reiterates the mechanism of long-distance skip communication. This refraction of HF signals back to Earth via the ionosphere gives rise to intercontinental HF radio communication and allows us to monitor international beacons. However, there are occasional and largely unpredictable disturbances of the ionosphere that interfere with HF communication. It is the nature of the ionosphere that affects the quality and distance of radio communication (Laster, 2000). Detailed explanation of ionospheric radio propagation is given in chapter 2.

1.1.2 The International Beacon Project (IBP)

For this study a radio beacon monitoring station was set up at the Hermanus Magnetic Observatory (HMO) to monitor international HF beacons. A radio beacon is a transmitter at a known location, which transmits a continuous or periodic radio signal on a specified radio frequency. The NCDXF, in cooperation with the IARU, constructed and operates a worldwide network of HF radio beacons on 14.10, 18.11, 21.15, 24.93 and 28.20 MHz (NCDXF, 2009). The beacons transmit according to a known timing sequence and calibrated power levels. Unlike HF propagation prediction models, which predict the expected performance of HF communications based on ionospheric variations due to sunspot activities, hours of the day and geographic location, the NCDXF/IARU International Beacon Project (IBP) assesses the current condition of the ionosphere by direct measurements.

There are at least two possible explanations for an apparantly dead band, either the propagation is poor or no one is transmitting (De Canck, 2006a). The IBP addresses the second of these possibilities by ensuring that reliable signals are

always on the air, around the clock, from fixed locations worldwide. So by listening to the beacons for three minutes, one can find out either when a particular band is open or which band has the best propagation to a particular part of the world (De Canck, 2006a). The network of 18 locations transmits in sequence for 10 seconds on each of the five bands, providing ninety ten-second transmissions from locations around the world every three minutes. Each transmission consists of the call sign of the beacon sent at 22 words per minute followed by four one-second dashes. The call sign and the first dash are sent at 100 W. The other three dashes are sent at 10 W, 1 W and 0.1 W, stepping downward in power with each dash. Every 10 seconds, the next beacon location listed on the transmission schedule starts transmitting, while the previously transmitting beacon moves up one band (from 14.10 MHz to 18.11 MHz, etc). After 50 seconds of transmission, a beacon cycle has cycled through all five bands, and remains silent for 130 seconds. At multiples of three minutes past the hour all 18 stations would have completed their transmission on 14.10 MHz and the first beacon on the transmission schedule starts another transmission cycle. More information about the IBP is given in chapter 2.

1.2 Aims of study

The project aims at setting up an automated monitoring station for international HF beacons at the Hermanus Magnetic Observatory, HMO (34.42°S, 19.22°E). The process involves extending the antenna system of the already existing HF radio transceiver by constructing and installing different antennas to receive the beacon signals. This includes the Inverted-vee dipole antenna and the MFJ-1778 G5RV multiband antenna. As a result, a suitable antenna was installed for the reception of the international beacon signals on all five HF bands. Appropriate beacon monitoring software was chosen and interfaced with the transceiver so as to monitor the beacons on all bands automatically and archive propagation reports for analysis.

An additional objective of this project was to create a web page on the HMO Space Weather website to communicate real-time HF propagation information to civilian and military users in terms that are easy to interpret and understand. To illustrate the application for the data gathered by the monitoring station, the beacon observation logs were analysed and used to validate the Ionospheric Communications

Enhanced Profile Analysis and Circuit (ICEPAC) prediction software.

1.3 Significance of study

The motivation behind this study lies in the fact that, even though HF radio communication cannot replace fixed and mobile telephony as the first communications option for the general public, it is a vital and irreplaceable long-distance wireless communications tool for amateur radio operators, organisations involved in emergency situations, as well as remote and military communications. It is often the most reliable means of communication when disaster strikes.

Since HMO recently became the International Space Environmental Service (ISES) Regional Warning Center (RWC) for Africa, this study contributes as an important product offered by the HMO space weather center. The real-time beacon monitoring station alerts users, through the internet, to unexpected radio propagation conditions. The propagation reports generated by the beacon monitoring station are useful to amateurs, commercial radio operators and the defence community to detect band openings on an individual frequency band. The real-time propagation reports indicates the strength of the signal and such information is vital, since it shows whether it is feasible to communicate on a particular frequency band or not. The propagation reports also help identify the frequency band which offers the best propagation to a particular part of the world. Finally, the beacon observation log files that are automatically saved can be used to validate HF propagation prediction models such as ICEPAC.

1.4 Thesis layout

The theoretical background for this study is presented in chapter 2. This is where the general structure of the ionosphere is discussed in terms of ionospheric layers and the processes that cause their build up, as well as its effect on HF propagation. Technical information regarding HF antennas is also given in this chapter, as well as the equipment used in setting up the beacon monitoring station. A detailed explanation of the procedures followed in setting up the monitoring station and its upgrade from a single band monitoring station to a multiband station is given. The details regarding the construction and installation of antennas, CI-V level converter and configuration of Faros 1.3 monitoring software are presented.

The results of this study are presented in chapter 4. The real-time propagation reports generated by the monitoring station are presented. A section on the validation of ICEPAC is also presented as an example of the application of the data that the monitoring station gathers. The overall summary of the project results

and the conclusion are given in chapter 5. Some possible future work that may be done to accomplish better results is suggested.

Chapter 2

Theory

This chapter outlines the theoretical background regarding the ionosphere and its use in HF radio propagation. The NCDXF/IARU International Beacon Project as well as the instruments/materials used in this study are described.

2.1 The Ionosphere

The main focus of this study is the ionosphere, a region which ranges from about 50 km to beyond 1000 km altitude within the Earth's atmosphere. The ionosphere is of major interest since radiation from the Sun ionises neutral atmosphere particles which results in radio waves sent into space being refracted and eventually reflected as they propagate through the ionospheric layers, depending on the prevailing conditions at the time of signal transmission.

The ionosphere is a weakly ionized plasma of net neutral charge (Brasseur and Solomon, 2005). It is often described as those regions of the upper atmosphere where charges, either positive or negative, are present in quantities large enough to influence the trajectory of radio waves. The existence of these charges results from the ionisation by the solar rays of the components of the overall neutral atmosphere, and therefore from photoionisation. This phenomenon was experimentally demonstrated around 1925 by different physicists, like Appleton, Barnett, Breit, Tuve and Marconi, in the wake of experiments conducted on the propagation of radio waves.

Atmospheric atoms and molecules can be ionized either by short wavelength solar radiation (ultraviolet and X-rays), or by precipitating energetic particles, mainly protons of solar origin as shown in equations 2.1 and 2.2:

$$X + h\nu \rightarrow X^{+} + e^{-} \tag{2.1}$$

$$X + p^* \rightarrow X^+ + p^+ \tag{2.2}$$

X is a neutral atom or molecule

$h\nu$ is the solar radiation energy

X^+ is the resultant positively charged ion

p^* is an energetic proton

p^+ is a free positively charged proton

These processes are the starting points for a series of reactions which determine the structure of the ionosphere. The ionosphere is divided into three layers, i.e the D, E and F layers. During daytime there may be four layers, namely the D, E, F1 and F2 while during the night only the F2 layer exists since, due to the continued radiative and dissociative recombination processes, the ionosphere has been depleted of free electrons. The ionosphere is an ever-changing medium. It does not allow the use of the same frequency throughout the year, or even over the course of a day. Figure 2.1 shows the definition of ionospheric layers based on the vertical distribution of electron density.

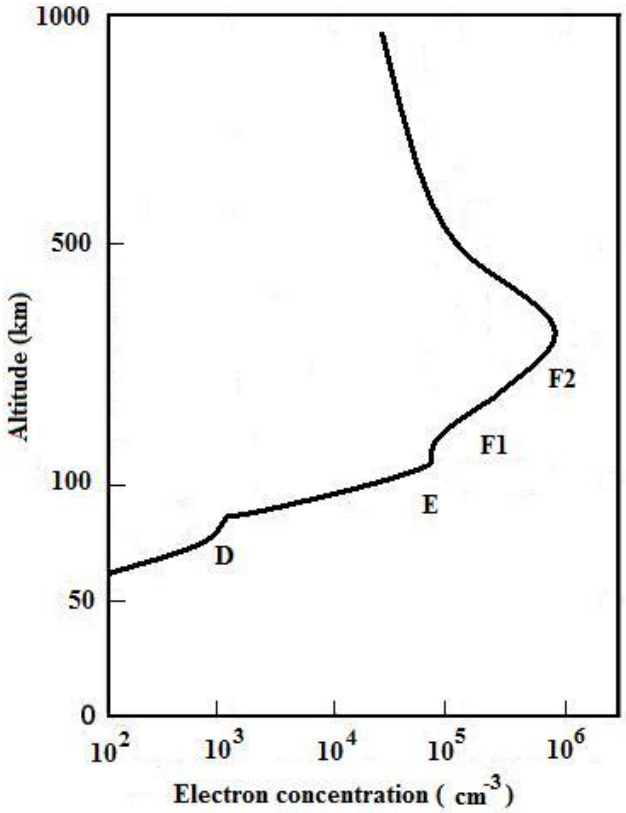

Figure 2.1: Definition of the ionospheric layers based on the vertical distribution of electron density (*after* Banks and Kockarts, 1973).

The ionosphere varies with the solar cycle, the seasons and during any given day. The E, F1 and F2 layers are the only layers that can reflect HF radio signals while the D layer is important because it absorbs the radio signals, especially those at lower frequencies and those signals with greater obliquity (Lusis, 1983).

The ionosphere is also sub-divided into three components called the lower, bottomside and topside ionosphere. The lower ionosphere is mainly composed of the D layer, whereas the E and F layers form the bottomside ionosphere starting at an altitude of about 90 km up to the height of maximum electron density. From the maximum electron density height up to beyond 1000 km is the topside ionosphere, a region of low and reducing particle density.

2.1.1 The D layer

The D layer extends to heights ranging approximately from 50 km to 90 km. Ionisation in this layer takes place due to low UV rays (wavelength = 121.6 nm) and X-rays (wavelength = 0.1 - 1 nm) from the Sun with wavelength. The ionised particles found in this layer are Nitrogen and Oxygen. The layer is present only during the daytime; as soon as the Sun's ionising radiation is no longer present, electrons and ions rapidly recombine to form neutral (un-ionised) gas and the D layer disappears. Ionisation in this region is the main cause of the absorption loss of the HF radio waves reflected at higher altitudes. The D layer electron concentration displays a pronounced seasonal variation (Maslin, 1987).

2.1.2 The E layer

The E layer lies just above the D layer at altitudes ranging from about 90km to 130 km. It consists of a normal E layer (E layer) and a sporadic-E layer (Es layer). The normal E layer is a regular layer with an electron concentration strongly dependent on the solar zenith angle and on the level of solar activity. The Es layer is (as its name implies) unpredictable and may form at any time of the day or night at altitudes of 90 to 130 km in the ionosphere (McNamara, 1991). Its electron densities are comparable to those of the F Layer. As a result, the Es layer can reflect high frequency waves which normally are supposed to be reflected by the F Layer.

2.1.3 The F layer

The F layer is the main region that makes long-distance HF propagation possible (Carr, 2001a). Atomic Oxygen is ionised by Extreme Ultraviolet (EUV) solar

radiation (10 - 100 nm), forming this layer. It is sub-divided into two portions called the F1 and F2 layers. The F1 layer extends from 130 to 210 km and the F2 layer extends from 180 to 300 km or higher. The distinction between these two layers does not hold during the night since F1 and F2 layers combine to form a single F layer that is less strongly ionised than during the daytime. Unlike the lower layers, the density of neutral atoms in the F layer is low enough so that ionisation levels remain high all day, decay is slowly after local sunset. Minimum levels are reached just prior to local sunrise.

2.1.3.1 Spread F

Dennison (2005) describes spread F as a diffuse effect caused by irregularities in the electron density of the F region. Its main effect is that of causing the received signal at the receiver to be a superposition of a number of waves that are reflected from different heights and locations in the ionosphere at slightly different times.

2.2 Ionospheric variations

Since the ionosphere's existence is directly linked to the radiation emitted from the Sun, as investigated by Simmons and Ace (1995), the rotation of the Earth around the Sun or changes in the Sun's activity, will result in variations in the ionosphere. These variations are of two general types: those which are more or less regular and occur in cycles and, therefore, can be predicted with reasonable accuracy, and those which are irregular as a result of abnormal behaviour of the Sun and, therefore, cannot be predicted. These ionospheric variations have important effects on radio wave propagation.

2.2.1 Regular variations

Regular variations that affect the extent of ionisation in the ionosphere can be divided into four main categories: diurnal, seasonal, solar cycle and latitudinal variations.

2.2.1.1 Diurnal variation

Diurnal variation is caused by the rotation of the Earth. The Sun rises and sets on a 24-hour cycle and, because it is the principal source of ionisation of the upper atmosphere, diurnal variation can be expected (Carr, 2001a). The electron

densities of the D, E and F regions increases until midday, and then they it decrease until evening.

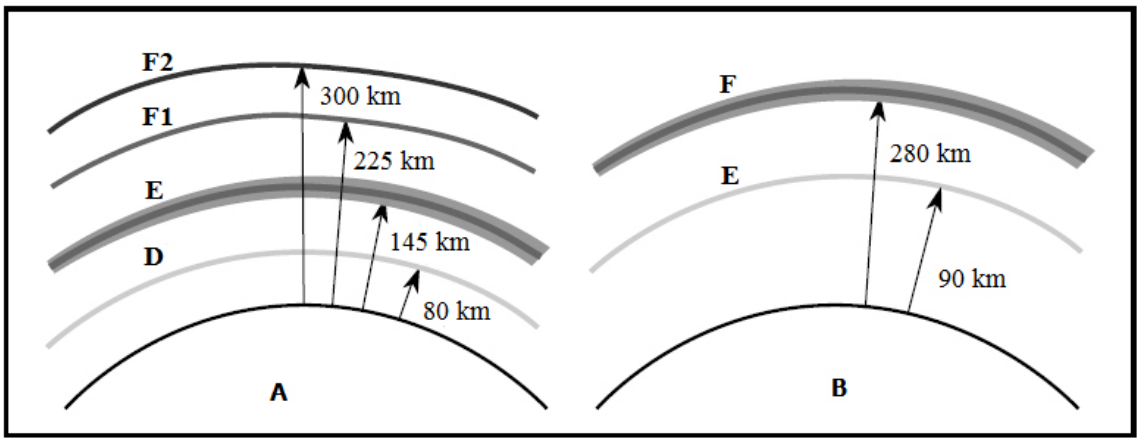

Figure 2.2: The ionospheric layers during the day (A) and night (B) (Laster, 2000).

Figure 2.2 shows that the D and E regions disappear (or reduce) at night and the F1 and F2 layers combine. As a result of higher absorption in the E and D layers, lower frequencies are not useful during daylight hours. In general, the F layers reflect higher frequencies during the day. In the 1 MHz to 30 MHz region, the higher frequencies (>11 MHz) are used during daylight hours, and the lower frequencies (<11 MHz) at night.

2.2.1.2 Seasonal variation

Seasonal variation is caused by the apparent north and south progression of the Sun. The Earth's tilt varies the exposure of the planet to the Sun on a seasonal basis. In addition, the Earth's yearly orbit around the Sun is not circular, but elliptical. As a result, the intensity of the Sun's energy that ionises the upper atmosphere varies with the seasons of the year. In general, the electon density in the D, E, and F1 layers are normally greater in summer, but the density in the F2 layer tends to be highest in winter, and less in summer. This is called the winter or seasonal anomaly (Davies, 1969).

2.2.1.3 Solar cycle variation

One of the most notable phenomena on the surface of the Sun is the appearance and disappearance of dark, irregularly shaped areas known as sunspots. According to Davies (1969), the exact nature of sunspots is not known, but it is believed that they are associated by violent eruptions on the Sun and are characterized by unusually strong magnetic fields. The solar activity associated with these sunspots

is responsible for variations in the ionisation level of the ionosphere. Sunspots can, of course, occur unexpectedly, and the life span of individual sunspots is variable; however, a regular cycle of sunspot activity has been observed. This cycle has both a minimum and maximum level of sunspot activity and lasts approximately 11 years. During periods of maximum sunspot activity, the ionization density of all layers increases. Because of this, absorption in the D layer increases and the critical frequencies for the E, F1, and F2 layers are higher. At these times, higher operating frequencies must be used for long-distance communication.

2.2.1.4 Latitudinal variation

Ionospheric latitudinal variation is due to the variation of the solar zenith angle with respect to latitude on the Earth's surface (McNamara, 1991). Polewards of the Tropics of Capricorn and Cancer the solar zenith angle can never be zero degrees in magnitude. This angle increases as latitude extends from the equator towards the poles.

2.2.2 Irregular variations

Besides the four regular variations, there are also irregular ionospheric variations that have an important effect on radio wave propagation. They can drastically affect communication capabilities without any warning since they are irregular and unpredictable (Rhodes, 1999).

2.2.2.1 Sporadic-E

Sporadic-E exists as cloud-like patches of unusually high ionization at heights near the normal E layer. The sporadic-E layer can form and disappear in a short time, at any time during either day or night. Sporadic-E often blanks out the reflections from higher ionospheric layers. It can also cause unexpected propagation of signals hundreds of kilometers beyond the normal range. Amongst other forms, it is often associated with auroral activity.

2.2.2.2 Sudden ionospheric disturbance (SID)

A sudden ionospheric disturbance occurs in conjunction with bright solar eruptions and result in intense ionisation of the D layer. As a result, radio transmissions on the lower part of the HF spectrum may become totally absorbed, which may lead to total failure of long-distance HF communication. These disturbances may

occur without warning and may prevail for any length of time, from a few minutes to several hours.

2.2.2.3 Ionospheric storms

Ionospheric storms are disturbances to the normal ionosphere, caused by disturbances in the Earth's magnetic field, which inturn are believed to result from particle radiation from the Sun. The most prominent effects of ionospheric storms are a turbulent ionosphere and very erratic sky wave propagation. Ionospheric storms affect the higher F2 layer, reducing its electron density. Lower layers are not affected appreciably by the storms unless the disturbance is great. As a result, the range of frequencies that can be used for communication on a given circuit is much smaller than normal, with skywave communication being possible only at the lower working frequencies. These storms may last from several hours to days and usually extend over the entire Earth (Rhodes, 1999).

2.3 Ionospheric HF radio propagation

Intercontinental broadcasting and communication on HF bands are achieved through ionospheric propagation using the skip phenomenon (as illustrated in Figure 1.1).

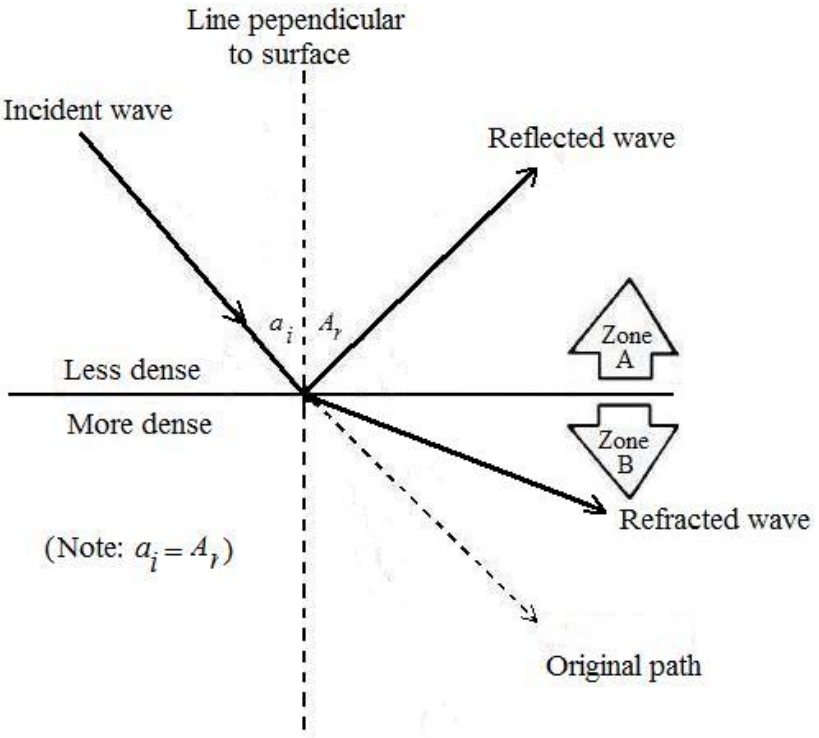

Figure 2.3: Refraction and reflection phenomenon between two media of different densities (*after* Carr, 2001a).

Under this type of propagation, the Earth's ionosphere acts as a reflecting mirror. Although the actual phenomenon is based on refraction, the appearance to the casual observer is that shortwave and high frequency (HF) radio signals may be reflected from the ionosphere (Carr, 2001a). Figure 2.3 shows the refraction and reflection between two mediums of different densities (zone A and zone B). a_i is the angle of incidence and A_r is the angle of reflection.

There are two principal ways radio waves travel from a transmitter to a receiver. One is by travelling along the surface of the Earth, known as the ground wave and the other is by refraction and eventual reflection from the ionosphere, known as the sky wave. As has been mentioned before, the propagation of HF radio waves over long distances is based on the reflection and refraction properties of the ionosphere. Due to the unstable nature of the ionosphere, radio wave propagation is subject to a number of variations that may either degrade or support the communication between two given locations.

2.3.1 Ionospheric refraction

Refraction of radio waves from the ionosphere is caused by the change in the velocity of an incident radio wave as it enters a new medium, as shown in Figure 2.3. The Appleton-Hartree equation (equation 2.3), describes the refraction of radio waves in the ionosphere. Sizun (2005) gives a detailed derivation of the Appleton-Hartree equation. Neglecting collisions in the plasma, the Appleton-Hartree equation is given by:

$$n^2 = 1 - \frac{X(1-X)}{(1-X) - \frac{1}{2}Y_T^2 \pm \left[\frac{1}{4}Y_T^4 + (1-X)^2 Y_L^2\right]^{\frac{1}{2}}} \tag{2.3}$$

where:

$$X = \frac{Ne^2}{\varepsilon_o m\omega^2} = \frac{\omega_p^2}{\omega^2} \tag{2.4}$$

$$Y_{L=}\frac{eB_L}{m\omega} = \frac{eB\cos\theta}{m\omega} = \frac{\omega_b \cos\theta}{\omega} \tag{2.5}$$

$$Y_T = \frac{eB_T}{m\omega} = \frac{eB\sin\theta}{m\omega} = \frac{\omega_b \sin\theta}{\omega} \tag{2.6}$$

and

θ is the propagation angle

N is the electron concentration of the medium

e and m refers to the charge and mass of the electron respectively

ε_o is the permittivity of free space

ω_p is the angular plasma frequency and $\omega_p = (Ne^2/\varepsilon_o m)^{1/2}$

ω_b is the angular electron frequency and $\omega_b = eB/m$

T and L refers to transverse (T) and longitudinal (L) components of the magnetic field B, compared to the normal of the electromagnetic wave with frequency ω.

As can be seen from equation 2.3 to 2.6, the refractive index depends on the transmission frequency and on the direction of propagation. The extent to which an incident radio wave is refracted by the ionosphere depends on the density of ionisation of the layer, the frequency of the radio wave and the angle at which the wave enters the layer (propagation angle).

Simmons and Ace (1995) clarified that to reflect a radio wave, the ionospheric layer must be thinner than one wavelength of the incident radio wave. But the ionospheric layers are often several kilometers thick, implying that ionospheric reflection is more likely to occur at low frequencies.

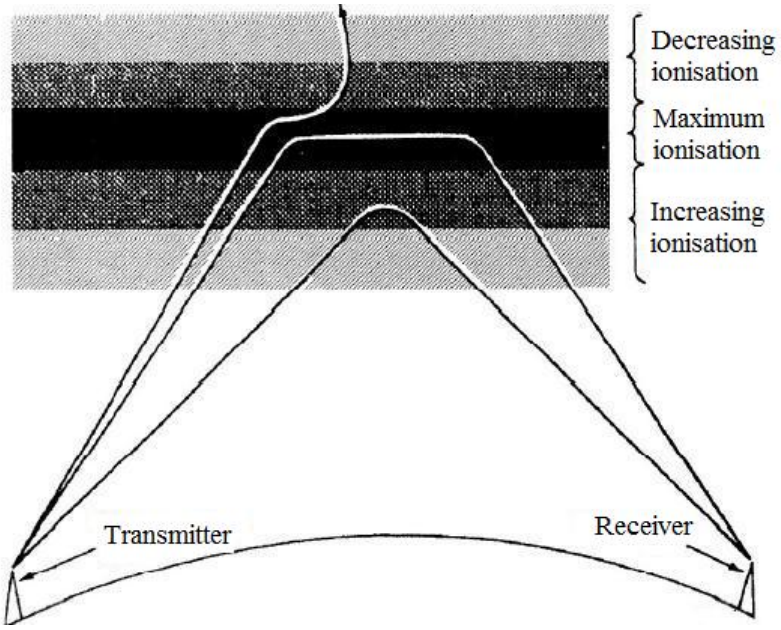

Figure 2.4: Effects of ionospheric density of radio waves (Simmons and Ace, 1995).

Sizun (2005) mentioned that in order to successfully propagate radio waves through the ionosphere, the frequency cannot be too low, as the wave would then be absorbed, nor too high, as reflection would no longer occur. As a result, two limiting frequencies exist, that are defined as the lowest useable frequency (LUF)

and the maximum useable frequency (MUF) respectively. Hence, for a frequency (f) to be usable for skywave communication, it must lie in the range:

$$LUF < f < MUF \tag{2.7}$$

The maximum 'take-off' angle (critical angle) for a given frequency to be reflected from an ionospheric layer is determined by the MUF of that layer.

2.4 Antenna fundamentals

This section outlines the theory behind the antennas that are presented in chapter 3 of this thesis. The operation of the HF choke balun is also discussed here.

A radio antenna can be defined as a device which converts an electric wave guided by a conductor into a free-space, unguided electromagnetic wave, and vice versa. Electrical energy is fed to the antenna via a transmission line, a conductor which passes electrical energy from one point to another. Transmission lines include coaxial cables, open-wire lines, twisted pair wires and single wire feeders. A matching device or balun is usually required to ease the abrupt transition between the guided wave and the free wave. The wave guided by the transmission line is radiated into space by the antenna (Orr and Cowan, 1990). The electromagnetic radiation from an antenna is made up of two components, the electric field (E) and the magnetic field (H).

2.4.1 Properties of antennas

The performance of an antenna can be affected by different parameters which can be adjusted during the design process. All antennas, regardless of their shape or size, have four basic characteristics: gain, reciprocity, directivity and polarization (Simmons and Ace , 1995).

2.4.1.1 Gain

According to Milligan (2005), gain is a measure of the ability of the antenna to direct the input power into radiation in a particular direction. The gain of an antenna depends entirely on the antenna design. Practically all antennas do not radiate uniformly in all directions, implying that there will be certain angles of radiation with higher gain than others. Antenna gain can also be described as the power output in a particular direction, compared to that produced in any direction

by an isotropic (omni-directional) radiator. Antenna gain is usually expressed in dBi, decibels relative to an ideal isotropic radiator.

2.4.1.2 Reciprocity

Various properties of an antenna apply equally, regardless whether the antenna is used for transmission or reception. Reciprocity is the ability to use the same antenna for both transmission and reception. The more efficient an antenna is for transmission at a certain frequency, the more efficient it will be as a receiving antenna for the same frequency. Figure 2.5 shows that when the antenna is used for transmission (view A), maximum radiation occurs at right angles to its axis. When the same antenna is used for reception (view B), its best reception is along the same path, that is, at right angles to the axis of the antenna.

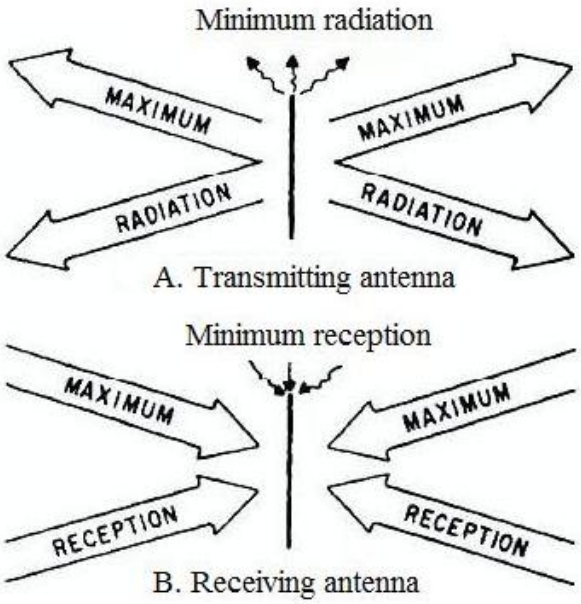

Figure 2.5: Diagram showing the reciprocity of antennas (Simmons and Ace, 1995).

2.4.1.3 Directivity

Directivity of an antenna is a measure of the antenna's directional characteristics. Directivity can be determined from the antenna radiation pattern. The numerical measure of directivity (D) is given by the ratio of the maximum power density (P) to the average power density (P_{av}) over the entire space, as shown in equations 2.8 and 2.9:

$$D = \frac{P}{P_{av}} \tag{2.8}$$

$$D(dBi) = 10\log\left(\frac{P}{P_{av}}\right) \tag{2.9}$$

2.4.1.4 Polarisation

Polarisation is defined as the orientation of the plane that contains the electric field component of the radiated waveform (Seybold, 2005). The polarisation of an antenna depends on the orientation of the antenna elements. Antennas with horizontally or vertically oriented radiation elements generate and receive horizontal and vertical polarisation respectively. Vertical and horizontal polarisations are examples of linear polarisation. Circular or elliptical polarisation is another type of antenna polarisation. According to Seybold (2005), circular polarisation is a linear combination of vertically and horizontally polarised waves with the appropriate phase.

2.4.2 Types of antennas

Antenna types include isotropic antennas, dipole antennas, aperture antennas, directive beam antennas and many other variations. The relationship between the wavelength at which the antenna is being operated and the actual length of the antenna is very important in antenna design. Specific dimensions must be used for efficient antenna operation.

2.4.2.1 Half-wave dipole antenna

The dipole antenna is one of the most important and commonly used types of radio frequency antennas.

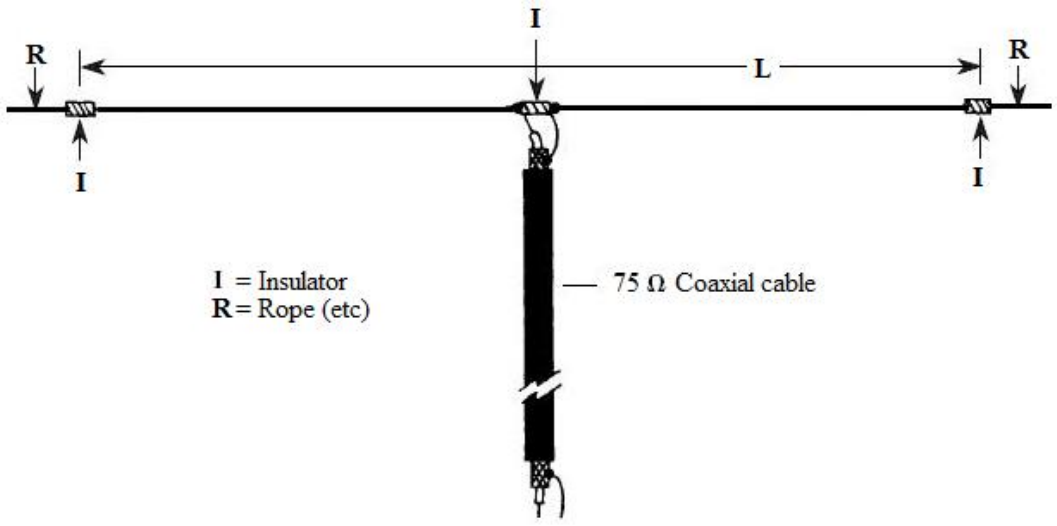

Figure 2.6: A simple half-wave dipole antenna in the flat-top configuration (Carr, 2001a).

The half-wave dipole is a balanced antenna that consists of two radiators, each a quarter wavelength long. Other lengths may be used, with different radiation patterns, gains and radiation resistances (the resistance to the current flowing into the antenna). The half-wave dipole antenna has a nominal broadside gain of 2.14 dB and reduced gain off the ends of the dipole (Seybold, 2005). The length (in meters) of a half-wave dipole in free space is given by:

$$L = \frac{150}{f} \tag{2.10}$$

In practice the antenna length calculated in equation 2.10 is too long. The average physical length is shortened by up to about 5 % because of the velocity factor (velocity of propagation of electromagnetic energy) of the wire and capacitive effects of the end insulators. Equation 2.11 therefore provides a nearly correct approximation of a half-wavelength dipole antenna.

$$L = \frac{143}{f} \tag{2.11}$$

where:

L is the length of the radiating element in metres; and

f is the operating frequency in mega hertz

2.4.2.2 Inverted-vee dipole

The half-wave dipole antenna can be installed in different configurations: namely, the flat-top (Figure 2.6), the inverted-vee (Figure 2.7); and inverted-L. The inverted-vee dipole is simply a half-wavelength dipole antenna with its center raised on a mast and the end points near the ground. The inverted-vee configuration was used in this study because the horizontal space requirement is less and only one tall support is required. Like a dipole, it is designed and cut for a specific frequency and has a bandwidth of 2 % above or below the design frequency (Rhodes, 1999). The inverted-vee antenna produces a combination of horizontal and vertical radiation because of its inclined sides. The apex angle, α, can be anything between 90° and 120°.

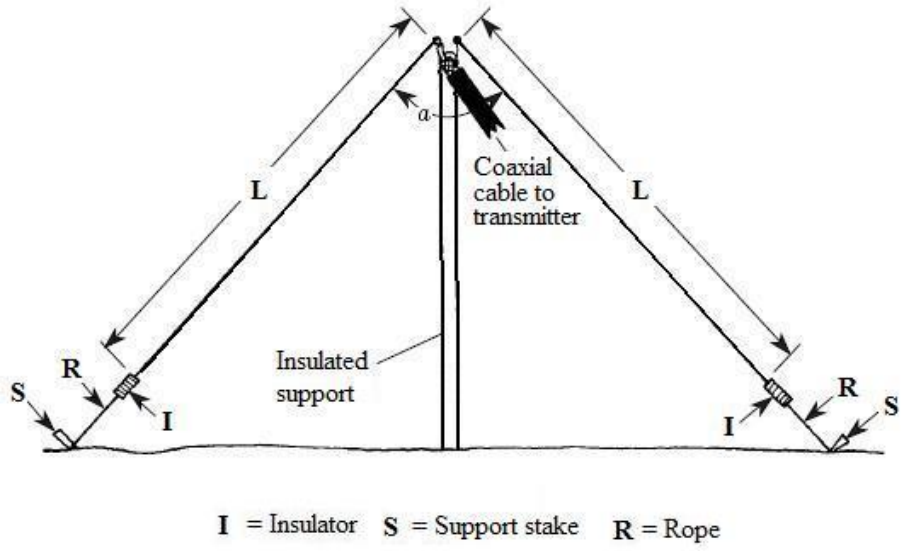

Figure 2.7: Inverted-vee dipole configuration (Carr, 2001a).

2.4.2.3 The G5RV multiband antenna

The Louis Varney G5RV antenna system incorporates a radiating element and a length of transmission line designed to present a correct impedance at a design frequency. The G5RV antenna is 3/2 wavelengths long at 14.15 MHz and this length, L, of 31.3 m was calculated using equation 2.12 (Varney, 1985).

$$L = \frac{150(n - 0.05)}{f} \tag{2.12}$$

where n represents the number of half-wavelengths in the antenna.

The G5RV antenna was originally designed to operate as a 3/2 wavelength center-fed antenna, but amateurs soon discovered it would offer reasonable performance on many other bands, hence its use as a multiband antenna (Varney, 1985). It consists of a 31.3 m radiating element with a 9.9 m 450 ohm matching section (also known as the ladder line) ending in an SO-239 coaxial connector. The 450 ohm matching section serves as a 1:1 transmission line transformer on 14.15 MHz. The standing wave ratio (SWR) is approximately 2:1 at 14 MHz. The same balanced line section acts like a transmission line impedance matching section on the other HF bands. The antenna also requires the use of an antenna tuner since the SWR of the G5RV is almost certainly not 1:1 on all the bands. An antenna tuner is an electronic device guarantees maximum performance on all bands by maximising power transfer. The G5RV antenna can be installed as flat-top, inverted-vee or inverted-L configurations. In this study the inverted-vee was used due to limited space for a flat-top configuration at the HMO where the antenna was installed.

2.4.3 HF choke balun

The word balun is a contraction of the words balanced and unbalanced. The primary function of the HF choke balun is to prevent the leakage of 'common-mode' currents, while making the transition from an unbalanced transmission line to a balanced load such as an antenna (Andress *et al*, 2000). While applying RF to a dipole antenna, two currents originate at the transmitter and flow on the inside of the coaxial cable:

- I1 flows through the central wire of the coaxial cable and from the transmitter goes up to the dipole antenna; and
- I2 flows on the inside part of the copper shield of the coaxial cable.

The two currents, I1 and I2 are equal and opposite and, therefore, cancel each other, so that no radiation takes place from these currents inside the coaxial cable. These two currents go onto the dipole antenna to be irradiated. However, part of the I2 current leaks out at the dipole feedline junction and comes back on the external side of the shield. This gives two currents on the shield namely I2 and I3. The value of I3 depends on the impedance value of the external side of the coaxial cable with respect to ground. If the impedance is high, I3 will find high resistance and its value will be low; if the impedance is low, the resistance will be low and the I3 value will be high. In this way I3 will radiate RF and the external side of the coaxial cable will radiate as a third wire of the dipole. As a consequence the antenna radiation pattern will be distorted. Figure 2.8 shows the current paths at a dipole feed point.

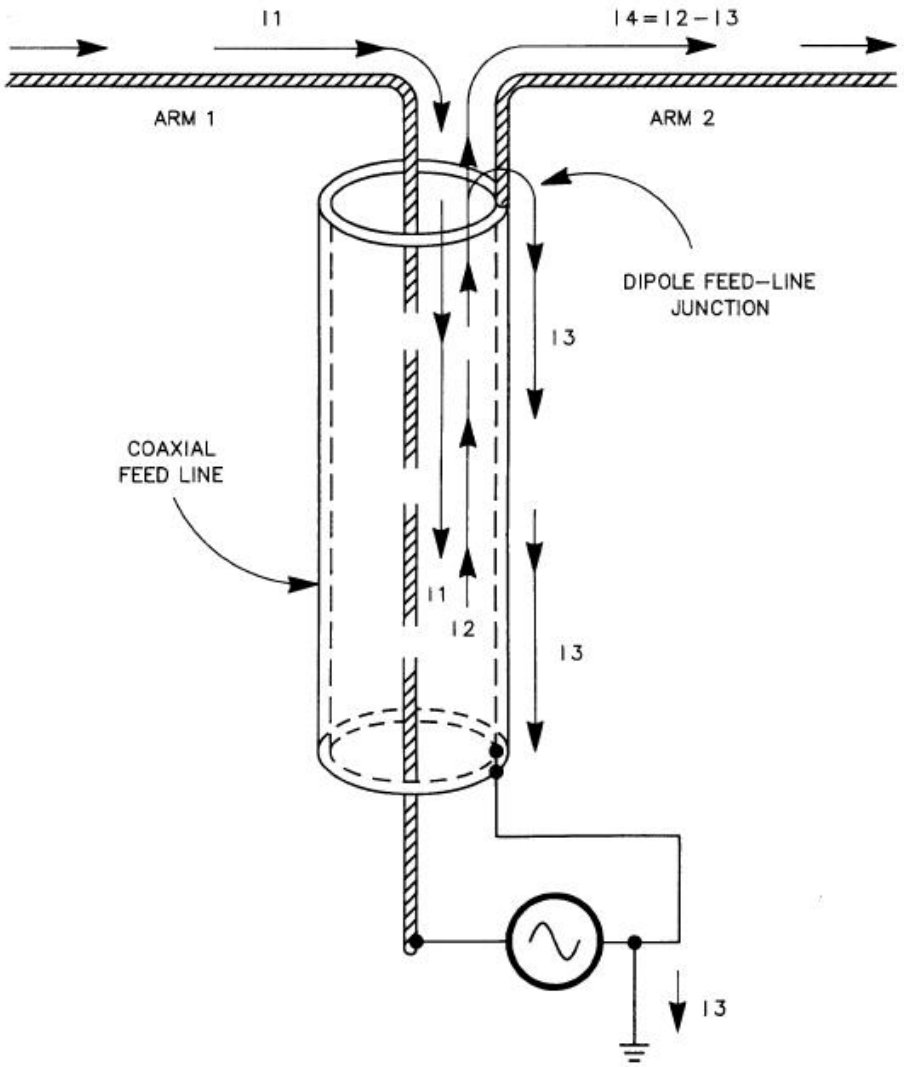

Figure 2.8: Illustration of the various current paths at a dipole feed point. The diameter of the coaxial cable is exaggerated to show currents clearly (Andress *et al*, 2000).

Using an HF choke balun, I3 will find a high impedance and its value will be very low. This will not disturb currents I2 and I4 that flow inside the coaxial cable.

2.5 HF radio transceiver (IC-728) and computer interfacing

The ICOM IC-728 is a radio transceiver designed to cover all nine amateur operating bands, 160 to 10 meters. This HF transceiver was used to set up the monitoring station as explained in chapter 3. It has a built in triple conversion 500 kHz to 30 MHz general coverage receiver. Output power is 10 to 100 watts continuous wave (CW) mode or 10 to 40 watts amplitude modulation (AM) mode

(Icom, 1992). The IC-728 can be connected by a Communication Interface - V (CI-V) level converter to a personal computer equipped with an RS-232C port. Icom CI-V controls the radio's frequency, operating mode, memory channels, etc. Up to four Icom CI-V transceivers or receivers can be connected through the Icom CI-V a personal computer equipped with an RS-232C port. Figure 2.9 shows the connections between the computer, CI-V level converter (CT-17) and four radio transceivers.

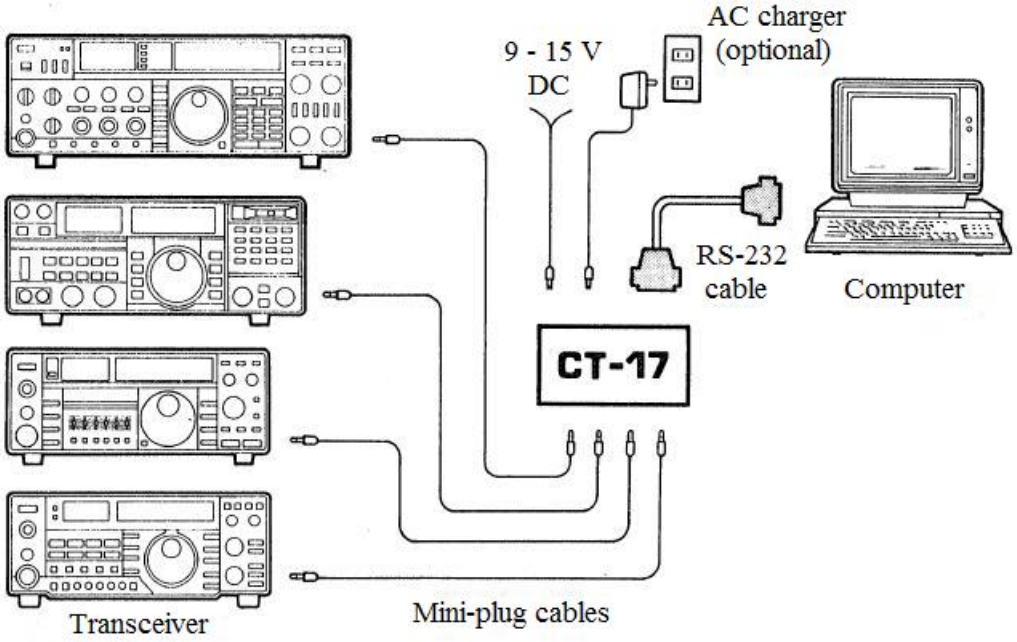

Figure 2.9: Diagram showing connections between computer, CI-V level converter (CT-17) and four radio transceivers. A single level converter can control up to four radio transceivers (Icom, 1992).

The set-up in Figure 2.9 allows the IC-728 transceiver(s) to exchange information with the computer and enhances computer-aided tuning of the radio transceivers using the CT-17 level converter.

2.6 The NCDXF/IARU International Beacon Project

The NCDXF/IARU International Beacon Project is a system of HF beacons around the world operating 24 hours a day, seven days a week transmitting on five HF bands, namely: 14.10, 18.11, 21.15, 24.93 and 28.20 MHz. The beacons transmit according to a known timing sequence and calibrated power levels. Each transmission consists of the call sign of the beacon sent at 22 words per minute followed by four one-second dashes. The call sign and the first dash are sent at 100 W. The other three dashes are sent at 10, 1 and 0.1 W, stepping downward in

power with each dash. With an accurate clock one can easily deduce which beacons are being monitored by using the information in Table 2.1. As was mentioned in chapter 1, the NCDXF/IARU International Beacon Project ensures that reliable signals are always on the air, around the clock, from fixed locations worldwide.

Call sign	**DX Entity**	**14.10**	**18.11**	**21.15**	**24.93**	**28.20**
4U1UN	*United Nations*	00:00	00:10	00:20	00:30	00:40
VE8AT	*Canada*	00:10	00:20	00:30	00:40	00:50
W6WX	*United States*	00:20	00:30	00:40	00:50	01:00
KH6WO	*Hawaii*	00:30	00:40	00:50	01:00	01:10
ZL6B	*New Zealand*	00:40	00:50	01:00	01:10	01:20
VK6RBP	*Australia*	00:50	01:00	01:10	01:20	01:30
JA2IGY	*Japan*	01:00	01:10	01:20	01:30	01:40
RR9O	*Russia*	01:10	01:20	01:30	01:40	01:50
VR2B	*Hong Kong*	01:20	01:30	01:40	01:50	02:00
4S7B	*Sri Lanka*	01:30	01:40	01:50	02:00	02:10
ZS6DN	*South Africa*	01:40	01:50	02:00	02:10	02:20
5Z4B	*Kenya*	01:50	02:00	02:10	02:20	02:30
4X6TU	*Israel*	02:00	02:10	02:20	02:30	02:40
OH2B	*Finland*	02:10	02:20	02:30	02:40	02:50
CS3B	*Madeira*	02:20	02:30	02:40	02:50	03:00
LU4AA	*Argentina*	02:30	02:40	02:50	03:00	03:10
OA4B	*Peru*	02:40	02:50	03:00	03:10	03:20
YV5B	*Venezuela*	02:50	03:00	03:10	03:20	03:30

Table 2.1: Beacon transmission schedule (NCDXF, 2009).

Since the beacons transmit at known times, it is easy to deduce which beacon one is hearing without copying the CW call sign.

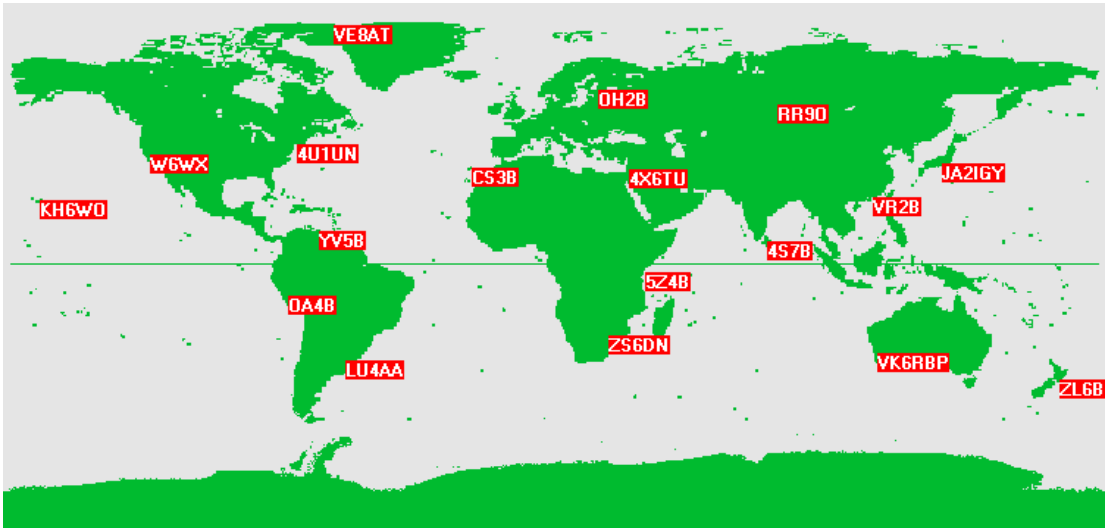

Figure 2.10: NCDXF/IARU beacon locations around the world (NCDXF, 2009).

Even a weak beacon signal may indicate a path with excellent propagation for stations using higher power and directive antennas, since the beacons are running 100 W to a vertical antenna. Figure 2.10 shows the locations of the beacons. In order to know which beacons are transmitting at any given time, one can either refer to the beacon transmission schedule (Table 2.1) or an automated beacon monitor, using a computer and a computer-compatible radio with appropriate beacon monitoring software.

2.6.1 Beacon monitoring software

Various software is available to help beacon listeners determine which beacon is transmitting on which frequency at any given time. These include Faros, VOAProp, ACE-HF, DXWatch and BeaconSee (NCDXF, 2009). Not only are they great for people who can't easily copy CW code at 22 words per minute, but they help identify the call sign of very weak beacons and that means that one no longer has to try to simultaneously look at a clock and a printed beacon schedule. These monitoring programs are available for different computers and operating systems. Most of these programs work offline and simulate beacon activity displaying simply the call sign and sometimes the location of the current beacon on a world map. Some applications using the VOACAP engine also predict the signal strength and reliability (Lane, 2005).

In this study the Faros 1.3 monitoring software was used. It is a complete NCDXF/IARU Beacon monitor system developed by Alex Shovkoplyas (VE2NEA) in 2006, capable of monitoring all 18 beacons on all bands automatically. It is intended for radio amateurs, short wave listeners and HF communication engineers, with many useful and practical features. Faros automatically detects the presence of the beacon, the short and long path, measures the signal-to-noise ratio (SNR) in dB, measures the percentage of time on a scale of 0 - 100 %, during which the signal is below the noise level (QSB index) and the signal propagation delay. Short path (SP) is the shortest distance that connects two locations on Earth and long path (LP) is the longest distance that connects two locations on Earth. Real-time results are displayed and data is accumulated in graphic charts and logs suitable for analysis and web publication.

2.7 HF propagation prediction models

Since sky waves propagate by reflection from the E and F regions of the ionosphere, they may suffer absorption when passing through the D region. As has

been mentioned, ionospheric conditions vary with time of day, time of year, and solar and geomagnetic activity. Various propagation prediction models exist in the form of software to predict the propagation path loss at different frequencies as well as the MUF, frequency of optimum transmission (FOT), LUF etc for propagation. Typically input parameters for such prediction programmes include time of day, month, transmitter and receiver position, frequency, sunspot number and possibly a geomagnetic index. The geomagnetic index is used in programmes which use special models for high latitudes. Due to the variations and uncertainty in ionospheric conditions, prediction programmes can give only statistical information.

In this study, ICEPAC (ITS, 2007) was used. It is an enhanced IONCAP (Ionospheric Communications Analysis and Prediction) model developed by the Institute of Telecommunications Sciences (ITS) in Boulder, Colorado, during the 1970s (Teters *et al.*, 1983). ICEPAC is a full system performance model for HF radio communications circuits in the frequency range of 2 to 30 MHz (Lane, 2005). It was designed to predict HF sky wave system performance and analyse ionospheric parameters. These computer-aided predictions may be used in the planning and operation of HF communication systems using sky waves, (ITS, 2007). The programme was developed with a much more elaborate high-latitude ionospheric model called Ionospheric Conductivity and Electron Density (ICED), taking the geomagnetic Q index as an additional input parameter. The computer programme is an integrated system of subroutines designed to predict HF sky wave system performance and analyse ionospheric parameters. ICEPAC predictions require user-defined input data, such as the year, month, day, frequency of operation, the type of antenna used, the transmitter power, the type of propagation prediction required and the man-made noise environment, among others.

2.8 Summary

The theoretical background to this study was outlined in this chapter. HF propagation was shown to be dependent on the varying ionospheric conditions. The chapter also explained fundamental principles underlying the materials and instruments used in setting up the real-time beacon monitoring station. Section 2.6 discussed the main tool used in this study, namely the NCDXF/IARU International Beacon Project. An explanation of the ICEPAC prediction model (used in chapter 4) was presented in section 2.7 of this chapter. This chapter therefore serves to provide the theory behind the procedure described in chapter 3 and the analysis of the results of the study in chapter 4.

Chapter 3

ZS1HMO monitoring station

This chapter gives a description of the procedure that was followed in setting up an IBP monitoring station at HMO (34.42^{o}S, 19.22^{o}E). ZS1HMO refers to the call sign of the Hermanus Magnetic Observatory where the station is operating. The task was broken down into two steps. Initially the single band station was installed, using the half-wave dipole and later it was upgraded into a multiband station (using the G5RV antenna), capable of automatically monitoring all the five IBP bands.

3.1 Single band set-up

The single band set-up was achieved by constructing and installing a half-wave dipole antenna in an inverted-vee configuration, constructing and installing the HF choke balun, choosing the appropriate beacon monitoring software; and monitoring the beacons on a selected IBP band (14 MHz). The IC-728 HF transceiver, shown in Figure 3.1, was used to receive the beacon signals.

Figure 3.1: Picture illustrating the IC-728 HF transceiver used to set up the beacon monitoring station.

3.1.1 Construction and Installation of the half-wave dipole antenna

The half-wave antenna was constructed using insulated copper wire as the radiating element. The antenna was cut according to equation 2.11, using 14.1 MHz as the design frequency. To determine the exact length at which the antenna has a reasonable SWR around its design frequency, an antenna analyser (designed by the MFJ Enterprises Inc.) was used. From equation 2.11, the antenna length was calculated to be 10.1 m and after the cut-and-try method using the MFJ 259 antenna analyser, the antenna length turned out to be 9.8 m. The half-wave dipole was installed in an inverted-vee configuration on a steel mast, 12 m high. This ensures highest antenna efficiency which occurs at heights greater than $\frac{1}{4}\lambda$. The apex angle was 108°, which also ensures better radiation resistance and efficiency since these fall rapidly at small apex angles.

Figure 3.2: The 12 m mast on which the inverted-vee dipole antenna was installed.

Figure 3.2 shows the 12 m steel mast on which the inverted-vee dipole antenna was installed. The picture also shows other dipole antennas not used in this project, but already installed on the mast in the inverted-vee configuration.

3.1.2 Construction of the coaxial HF choke balun

The inverted-vee dipole antenna was fed by a coaxial cable (RG-58). Since a coaxial cable (an unbalanced line i.e one that has just one conductor and a ground) was used to feed a dipole antenna (a balanced line i.e one which has two conductors with two equal currents in opposite directions), an HF choke balun was constructed to convert between balanced and unbalanced electrical signals that exist between the transceiver and the antenna as explained in section 2.4.3. This was constructed by winding coaxial cable into a coil of 10 turns of 15.2 cm diameter on a PVC ring as shown in Figure 3.3. The design follows the suggestion by Varney (1985) that the balanced to unbalanced effect, caused by the direct connection of coaxial feeder cable to a balanced antenna, can be reduced by winding the coaxial cable into a coil of 8 to 10 turns, about 15 cm in diameter, immediately before the point of connection of the coaxial cable to the base of the matching section. In our case this was at the end of the parallel wires at the base of the antenna mast.

Figure 3.3: Constructed HF choke balun, showing the coaxial cable wound on the PVC ring.

3.1.3 Monitoring software

Faros 1.3 was chosen to monitor the beacons automatically because of the following useful and practical features:

- Continuous monitoring of the 18 NCDXF/IARU beacons on the five HF bands. The user has the choice to activate any combination of the bands, from only one band to all five.
- Even with heavy interference and noisy environments, the programme still automatically detects the presence of the beacon signals.

- Three parameters are recorded : the signal to noise ratio (SNR), the percentage of time on a scale of 0 - 100 %, during which the signal is below the noise level (QSB index), and the propagation delay of the signal. In addition, Faros calculates the "evidence" i.e the measure of probability that the received signal was transmitted by the IBP beacon, on a logarithmic scale with detection threshold of evidence = 1.

- It identifies whether the received signal arrived via short path (SP) or long path (LP) by precisely maintaining a software-coordinated universal time clock (UTC).

- The real-time display informs the user instantly about the current band conditions.

- The software maintains a long-term history of beacon observations. This occurs daily via two charts (SNR and Path) and one numerical data log file.

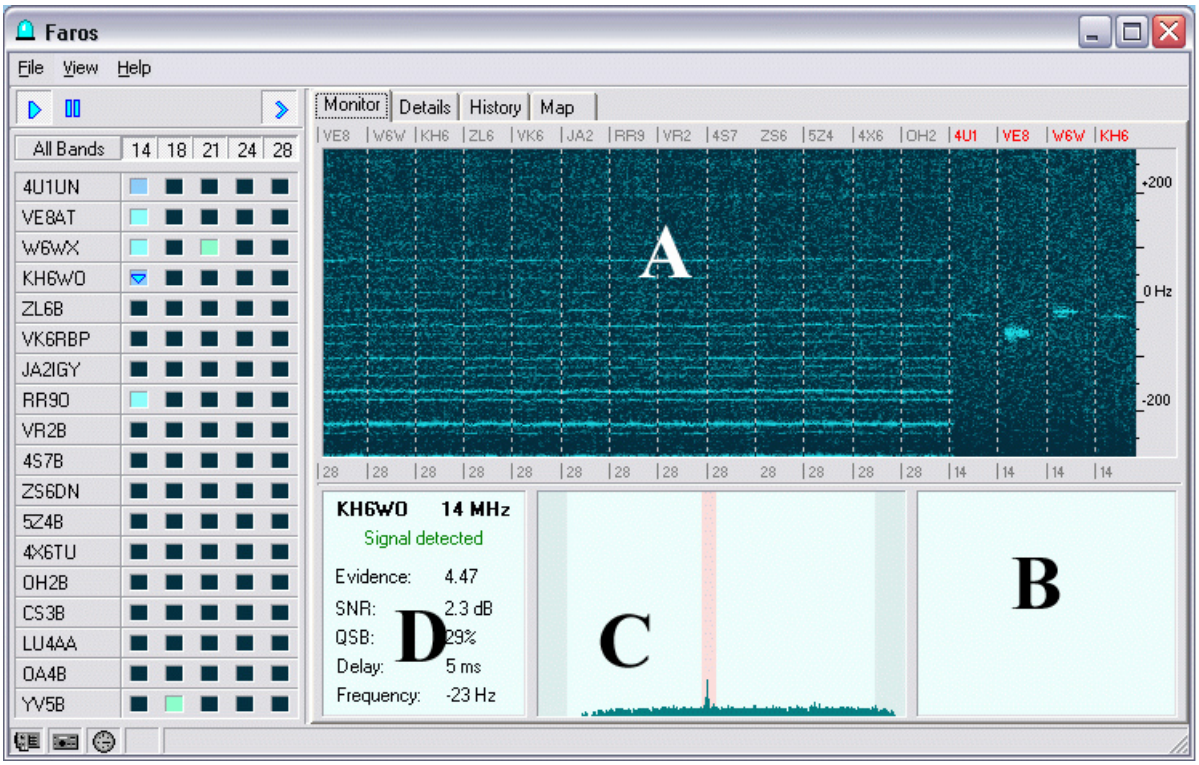

Figure 3.4: Faros 1.3 monitor page. The details, history and map pages can be accessed also.

Figure 3.4 shows the Faros 1.3 monitor page which consists of three parts: the waterfall display (view A), the spectral display (view C), and the observation results display (view D). The waterfall is split into ten-second time slots according to the beacon's transmission schedule. Above each time slot is an abbreviation of

the beacon call sign, which is shown in red when the beacon is detected. Below the time-slots is the monitored band label. The waterfall display shows how Faros filter and recognise the beacon signals out of noise. The bottom left panel (view D) displays the numerical results of the last observation. If the beacon was not detected, then the text is shown in grey. The bottom middle panel (view C) is the spectral window, giving graphical plots of the noise level and a possibly detected beacon signal. The bottom-right panel (view B) has been reserved for future use (De Cank, 2006a).

3.1.4 Monitoring the beacons on single band

The installed inverted-vee dipole antenna was connected to the HF radio transceiver (IC-728). Faros 1.3 beacon monitoring software was configured to monitor the international beacons on 14.1 MHz. The software configuration included defining the monitoring station's coordinates which are used to compute signal time delays and to show the observer's location on the world map. A standard stereo (audio) cable was used to input the audio signal from the radio transceiver to the computer.

Accurate UTC time is most critical for the correct operation of the software. Faros does not rely on the PC clock itself; it maintains its own UTC clock in the software. A fast internet connection to the HMO time server was used for the software from which to query time. Faros was also configured to save SNR plots (history files) and path files automatically every three minutes. A web page was created, on the HMO space weather website (ISES Regional Warning Centre for Africa), http://spaceweather.hmo.ac.za, where the SNR, SP/LP files were uploaded. These files were updated every 3 minutes and served as a real-time indicator of HF propagation conditions on 14.1 MHz.

3.2 Multiband set-up

Multiband set-up involved the installation of the MFJ-1778 G5RV multiband antenna, construction and installation of the Communication Interface - V (CI-V) level converter and configuration of Faros 1.3 to monitor the beacons on all five IBP bands, 14.1, 18.11, 21.15, 24.93 and 28.2 MHz.

3.2.1 Installation of the G5RV multiband antenna

The G5RV multiband antenna was installed in an inverted-vee configuration on the 12 m high HMO mast shown in Figure 3.2. The inverted-vee configuration

was the best option given the limited space to install the antenna. Special care was taken to isolate the radiating elements, as well as the matching section of the antenna from the steel mast because the antenna should be at least 15.24 cm away from any electrical conductor, including the mast itself. To achieve this isolation, plastic insulators were constructed and installed on the mast. Figure 3.5 shows the installation of the G5RV antenna with its matching section (ladder line) being tied to the end of the installed plastic insulators, 50 cm away from the aluminium conductor supporting the plastic insulators.

Figure 3.5: G5RV antenna installation on the 12 m mast.

The installation has an apex angle of 108° and allows the G5RV's matching section to drop symmetrically and vertically from the centre insulator for 9.9 m while being held away from the conductive steel mast. Since the G5RV is a balanced antenna fed with a balanced 450 ohm matching section that terminates in an SO-239 connector, a choke balun (construction description in section 3.1.2), was installed at the coaxial to feed point connection. This was done to reduce or eliminate parallel currents on the outside of the coaxial shield and hence prevent or reduce radio frequency interference (RFI), radio frequency (RF) feedback and other effects of excessive RF in the monitoring station.

3.2.2 Construction and installation of the CI-V level converter

Multiband monitoring of international beacons using Faros requires the HF transceiver to be able to communicate with the computer so that Faros can send commands to the transceiver to change its band automatically after each beacon transmission slot. In order to connect the ICOM IC-728 HF transceiver to the computer for remote control, a CI-V level converter that is capable of converting RS232 signal levels to ICOM's 5 V open collector bus line, was constructed. The level converter allows the configuration of Faros to monitor any combination of bands. Without the level converter, only one band can be monitored. The level converter construction was based on Icom's CT-17 level converter design (Icom, 1986). Figure 3.6 shows the circuit diagram for the construction of the level converter.

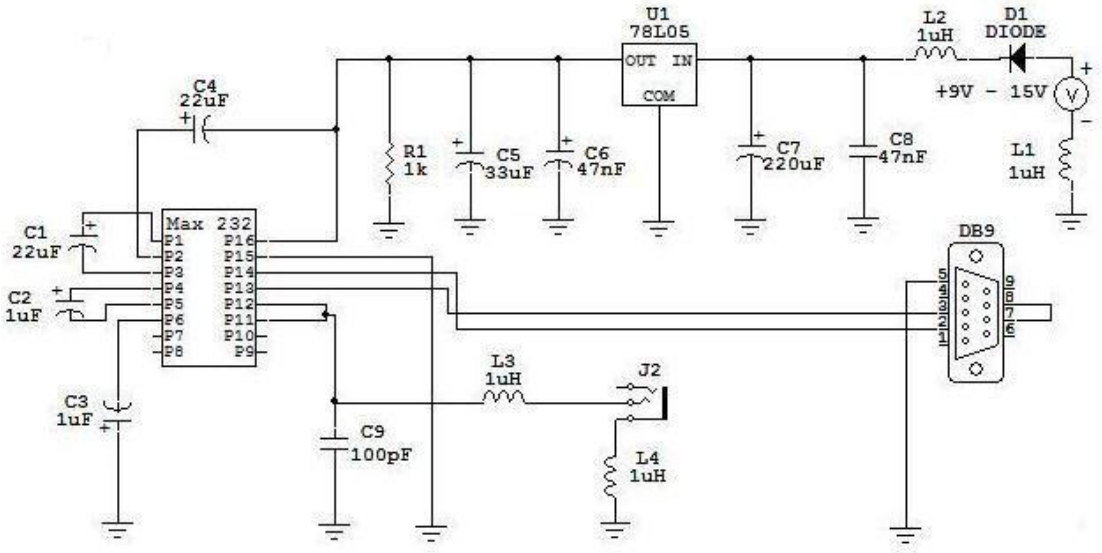

Figure 3.6: CI-V level converter circuit diagram.

The converter design is based around the Maxim 232 IC (Max232), which is a complete RS-232 interface. The chip uses four external capacitors, i.e, C1, C2, C3 and C4, which are part of the internal charge pump that generates +/-10 V from the single +5 V supply. The + 5 V power supply in the circuit diagram uses a 78L05 regulator that takes an input of +12 V from an external power supply and regulates it down to the +5 V needed to power the Max232 chip. The design also uses 1μH inductors, i.e, L1, L2, L3 and L4, to filter the power and radio data line. The DB 9 female connector, which connects to the computer's serial (COM) port, has pin 7 (RTS) and pin 8 (CTS) connected to each other. This signal return was done so that a computer programme that demands to see certain control signals on the COM port will indeed see them. On J2 (CI-V bus),

the open collector transmitter data output (pin 12) is directly wired to the receiver data input (pin 11), implying that all data are carried on a single line regardless of the data direction (computer-to-radio or radio-to-computer). The constructed CI-V level converter is shown in Figure 3.7.

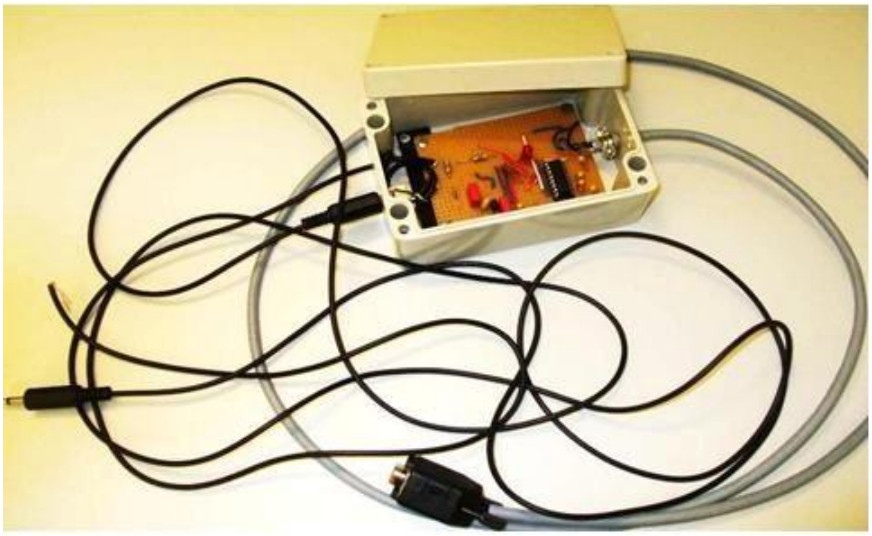

Figure 3.7: Constructed CI-V level converter, illustrating the CI-V jack that connects to the transceiver and the DB9 connector that connects to the computer's COM port

As a precautionery measure, the level converter was tested using a digital oscilloscope before installation. This was so as to avoid damaging the transceiver's CI-V port and to confirm proper signal conversion. The level converter was connected to the computer's COM port and powered. The programme hyperterminal in Windows was used to establish communication between the computer and the transceiver. When the key "C" on the computer keyboard in the hyperterminal window was pressed, this was pumped out of the serial port as a RS-232 signal level and seen as a waveform on the digital oscilloscope as shown in Figure 3.8(A). After conversion by the level converter, the RS-232 signal was seen as a transistor-transistor logic (TTL) signal on the oscilloscope as shown in Figure 3.8(B). This proved that the CI-V level converter was processing the signal conversion accurately, and the installation could go ahead.

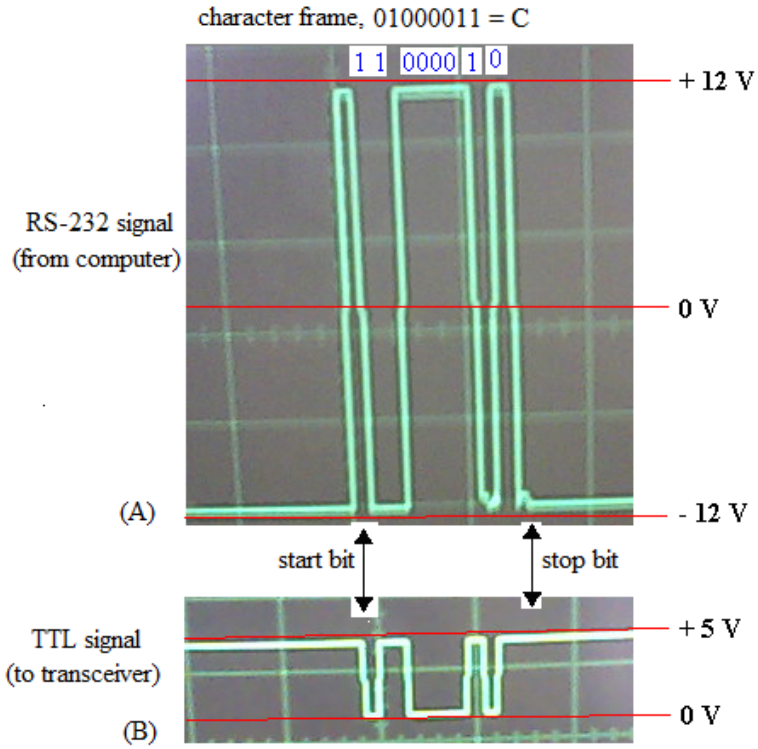

Figure 3.8: Oscilloscope traces showing RS-232 to TTL signal level conversion performed by the CI-V level converter.

The level converter was installed and Faros was configured for computer-aided tuning of the HF transceiver to enhance multiband beacon monitoring. The data format that was specified in Faros is 1200 bits per second (bps) 8-N-1 without flow control. This means that the computer communicates with the transceiver at a rate of 1200 bps and that each byte will have 8 data bits, with no parity bit, and only 1 stop bit. This set-up allows the transceiver to switch from one frequency band to another as instructed by the monitoring software through the commands sent via the CI-V level converter.

3.2.3 Multiband beacon monitoring

The G5RV multiband antenna, HF choke balun, CI-V level converter and the HF transceiver (IC-728) were connected to give a full IBP multiband monitoring station. Faros 1.3 was configured for multiband operation. The configuration of Faros followed the one in section 3.1.4, with additions on the enabled CI-V interface control, which allows the transceiver to scan through the five IBP bands, one after the other. As a result, the software spends 3 minutes on each band, implying that it takes 15 minutes to monitor all the five bands.

During the monitoring process each measurement is automatically saved on the signal charts (SNR and path files). The signal charts are available on the HMO space weather website (http://spaceweather.hmo.ac.za) as a real-time indicator of propagation conditions on 14.10, 18.11, 21.15, 24.93 and 28.2 MHz. The files update every three minutes. Figure 3.9 below shows the set-up of the multiband monitoring station.

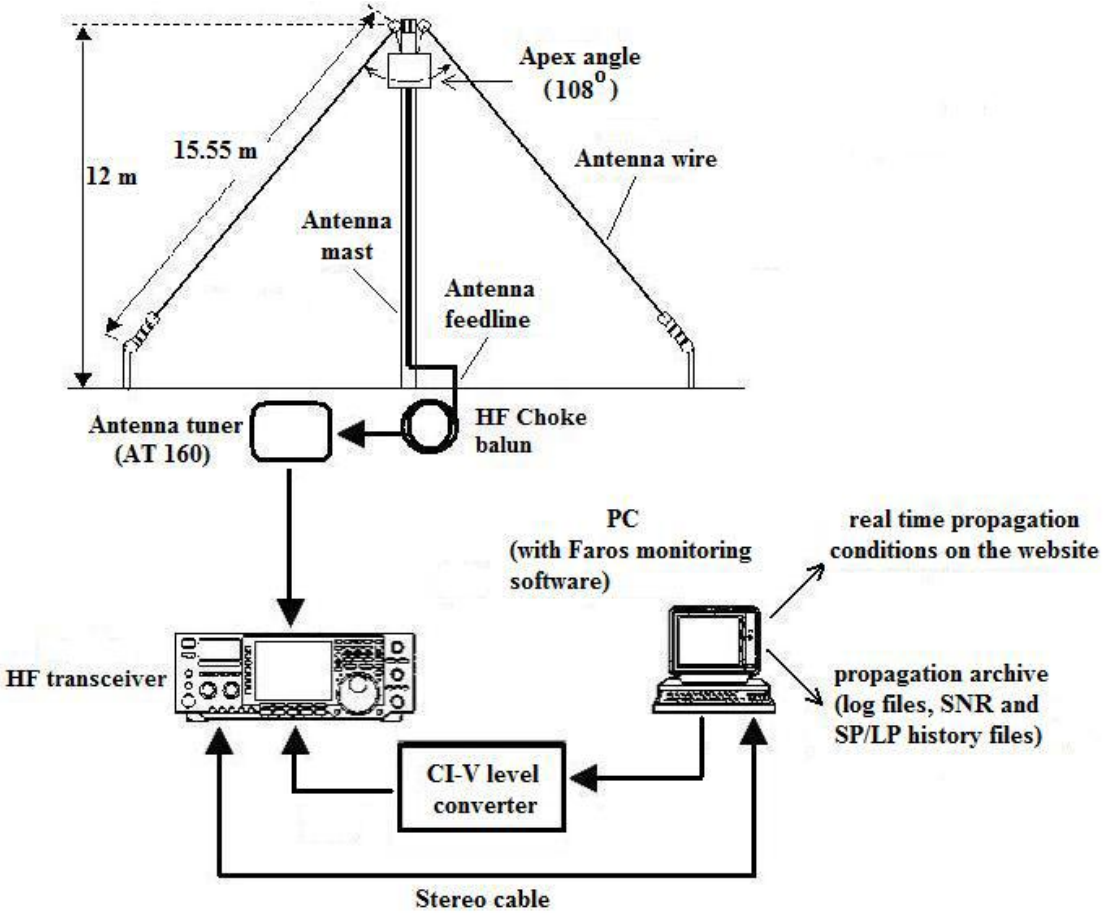

Figure 3.9: Diagram showing the complete set-up of the multiband monitoring station.

In Figure 3.9 the G5RV multiband antenna receives beacon signals on the five IBP bands. The HF choke balun, at the end of the antenna matching section, provides a proper current path between the antenna (balanced line) and coaxial cable (unbalanced line). The AT-160 antenna tuner is connected between the balun and the HF transceiver to minimise losses due to impedance mismatch and hence to maximise power transfer. The CI-V level converter connected between the transceiver and PC converts the TTL (5V) level of the CI-V interface to the RS-232 level of the PC and hence allows the transceiver to be remotely controlled by Faros software on the PC. The stereo cable takes the beacon audio signals from the transceiver and inputs them to the PC soundcard. Faros monitoring

software takes the input beacon audio signals from the soundcard and measures the following parameters: SNR, QSB, delay and evidence.

Chapter 4

Results

The real-time beacon monitoring station (ZS1HMO) was successfully set-up at HMO, as outlined in chapter 3. This chapter presents some beacon reception results. The monitoring station measures three parameters: SNR, QSB index and delay (as explained in chapter 3, section 3.1.3). In addition, the station calculates the 'evidence' for each beacon measurement. The quality of communication between a transmitter and a receiver depends on the SNR detected by the receiver. In this study therfore, the parameter SNR is used as the measure of the quality of the communication over the observed path.

4.1 Real time propagation conditions

This section presents the results and explains the real-time signal plots that are produced by the ZS1HMO monitoring station. The signal plots are available on the HMO space weather website (http://spaceweather.hmo.ac.za) as indicators of real time propagation conditions. The single band signal plots from 01 September 2008 to 15 December 2008 and the multiband signal plots from 16 December 2008 to 01 June 2009 date are available on the website. It is important to note that the monitoring equipment is sometimes used for normal HF activities, so no data is collected during these periods.

4.1.1 Single band signal plots

The single band beacon measurements, made daily by the monitoring station, were very important and useful for showing the real-time HF propagation conditions on 14.1 MHz. The signal plots in Figures 4.1 and 4.2 show the history of observations for a full day (2 October 2009). The signal plots are updated each time a beacon observation is made, as shown by the colour blocks on the signal plots. Since

it takes three minutes to listen to and record all 18 ten-second transmissions from the 18 IBP beacon transmitters, the signal charts are also updated every 3 minutes to show the latest propagation properties live on the internet. Each beacon observation in Figure 4.1 shows the strength of the received signal as depicted by the signal to noise ratio (SNR) on the colour legend. For each beacon observation made, in Figure 4.1, the signal path is recorded accordingly as shown in Figure 4.2.

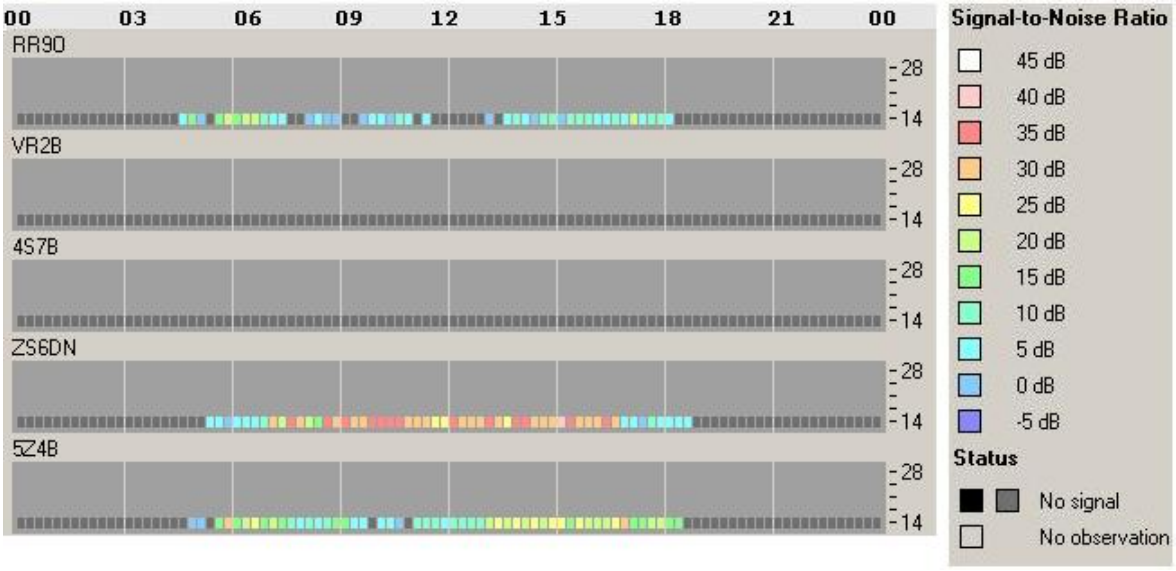

Figure 4.1: Extract from the single band SNR plot of 2 October 2008, showing real-time monitoring of five of the 18 IBP beacons.

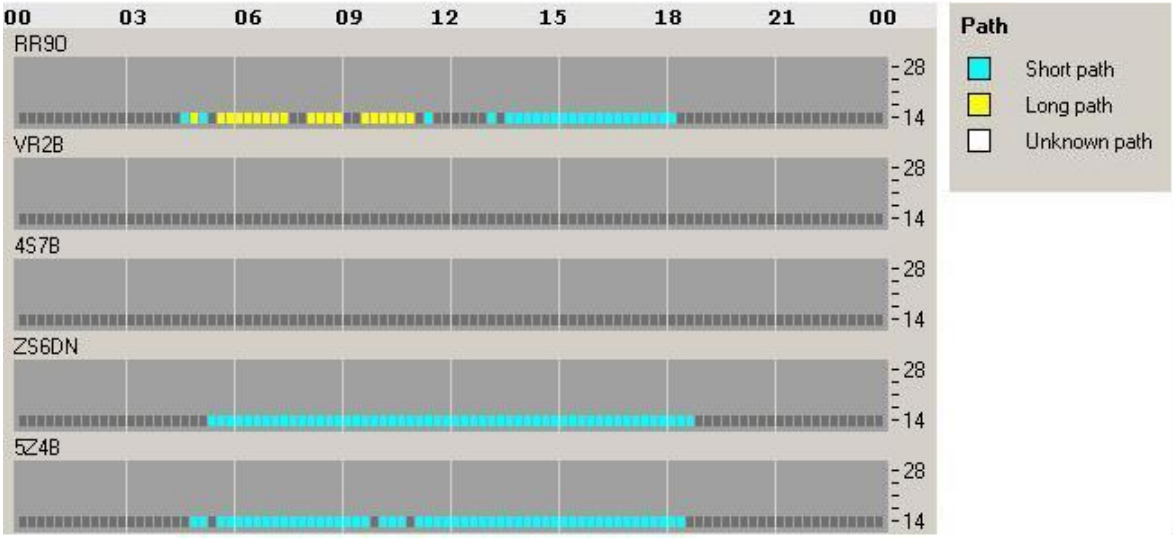

Figure 4.2: Extract from the single band path plot of 2 October 2008, showing real-time monitoring of five of the 18 IBP beacons.

4.1.2 Multiband signal plots

Multiband beacon reception reports are currently available on the HMO space weather website, showing propagation conditions on 14.10, 18.11, 21.15, 24.94 and 28.2 MHz. Signal plots on the internet are updated every 3 minutes. Figure 4.3 shows a sample of the SNR measurements for 12 January 2009 and Figure 4.4 shows the corresponding signal path. The quality of communication between beacon transmitter locations and ZS1HMO station is indicated by the measured SNR. The higher the SNR measured by the ZS1HMO monitor station, the better the quality of radio commnunication between the particular transmitter and ZS1HMO station.

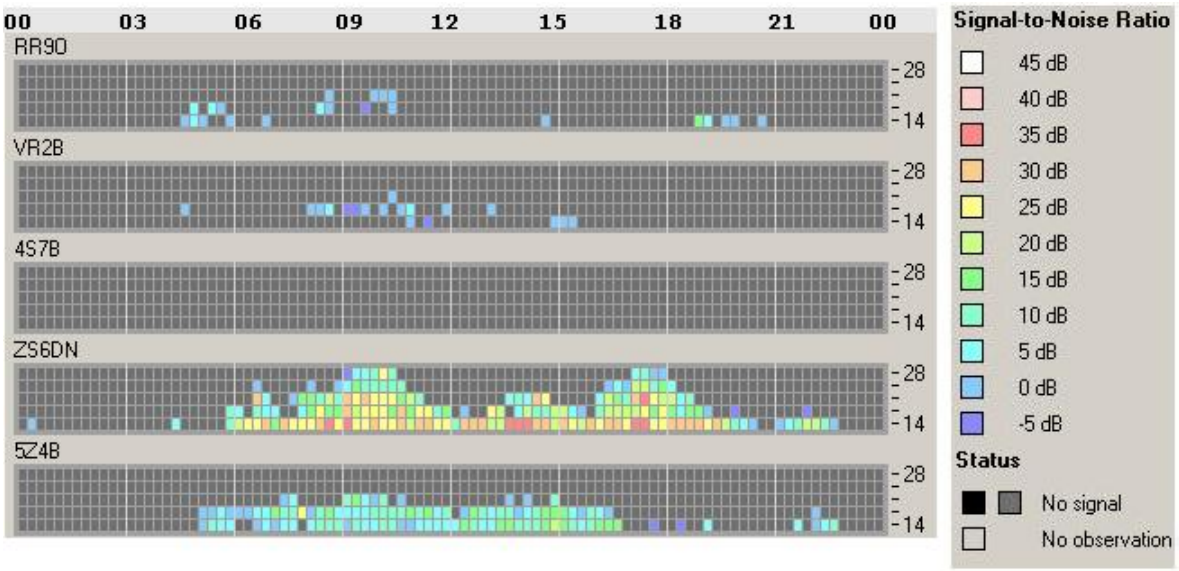

Figure 4.3: Extract from the multiband SNR plot of 12 January 2009 showing real-time monitoring of five of the 18 IBP beacons.

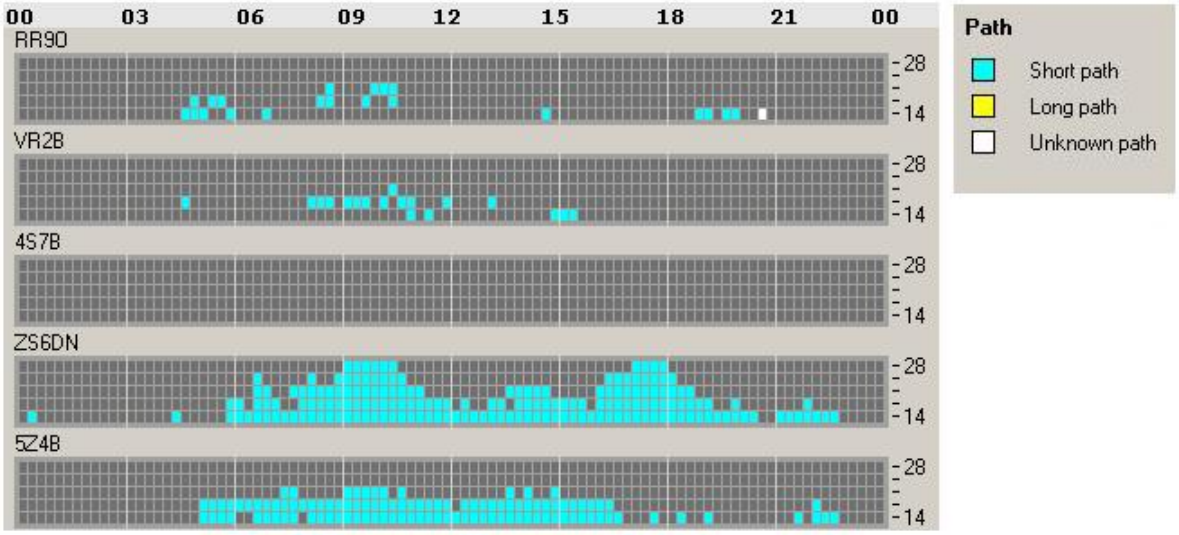

Figure 4.4: Extract from the multiband path plot of 12 January 2009 showing real-time monitoring of five of the 18 IBP beacons.

4.2 Worldwide beacon reception

In this section, a few observations that are part of the larger archive that is being collected at the ZS1HMO monitor station are presented. Because of the variability of the ionosphere and the propagation geometry, HF propagation is characterised by the need to select a suitable operating frequency as frequently as the ionosphere changes. There are also unpredictable irregular ionospheric variations that have a degrading effect and cannot be compensated for at any time. These, at times, disrupt HF communications. However, monitoring IBP beacons provides the opportunity to observe how HF propagation varies, by considering the strength of the signal received relative to the noise level, i.e, SNR. So if a beacon has a large, positive SNR, the frequency band will be good for communication (Troster and Fabry, 1997).

Figures 4.5, 4.6, 4.7, 4.8 and 4.9 show samples of beacon observations, recorded on the 6, 7 and 8 January 2009 from five continents: Africa, Asia, Europe, North America and South America. The observations at each frequency (14.1 MHz - 28.2 MHz) show the variation in signal quality received from the five continents considered. Archiving this information over a longer period will provide a valuable database from which future HF propagation prediction models can be built.

4.2.1 Africa

There are three beacons transmitting from or near Africa: ZS6DN in Pretoria, South Africa (25.90°S, 28.27°E); 5Z4B in Kariobangi, Kenya (1.24°S, 36.88°E) and CS3B in Santo da Serra, Madeira (32.72°N, 16.80°W). The circuit path considered here is ZS6DN - ZS1HMO, which has a short path of 1 284 km and a long path of 38 740 km.

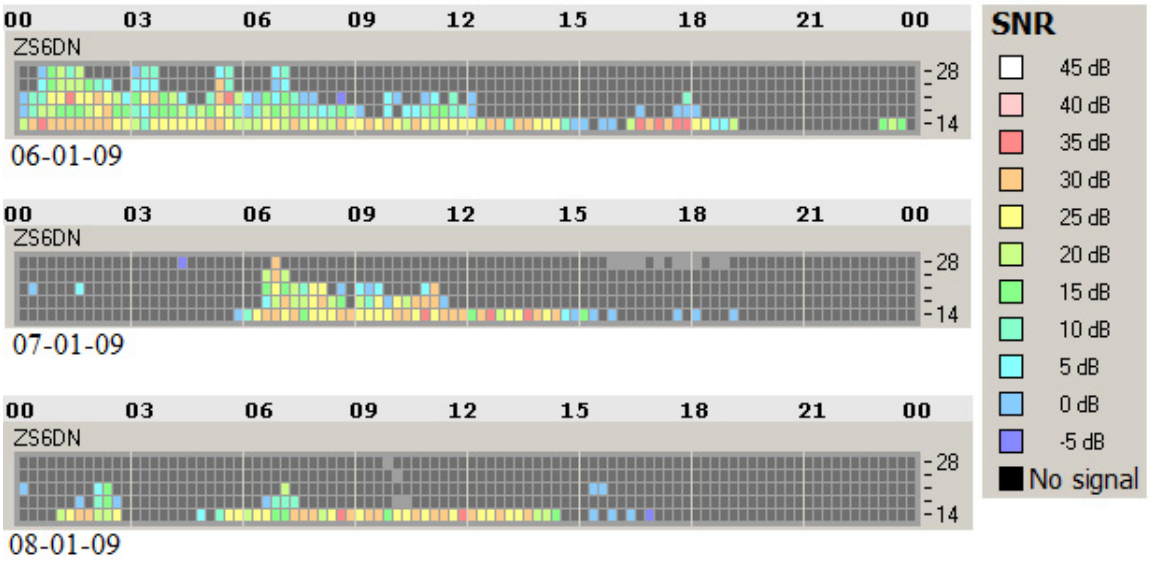

Figure 4.5: Reception of beacon signals from ZS6DN, South Africa.

The ZS6DN beacon is the closest of all the IBP beacons to the ZS1HMO monitor station. In Figure 4.5, daytime propagation (04 UT to 16 UT) shows SNR values reaching their lowest at sunset, approximately 16 UT, in step with reduction of ionisation in the ionosphere, which occurs with low solar radiation as sunset approaches. Strong night time multiband propagation openings with SNR of up to 40 dB were observed between 00 UT and 04 UT on 06-01-09. This was probably the result of reflection by sporadic-E (Es) layers at the circuit midpoint. The SNR levels were high and occurred for long durations, suggesting that the Es clouds had large horizontal extent, as investigated by McNamara *et al*, (2008). The opening of the 28.2 MHz band is usually linked to sporadic E activity (De Canck, 2006a), which can support transmission paths up to 2 100 km for single-hop propagation.

4.2.2 Asia

Five beacons transmit from Asia: VR2B in Hong Kong (22.27°N, 114.15°E); RR9O in Novosibirsk, Russia (54.98°N, 82.90°E); 4X6TU in Tel Aviv, Israel (52.05°N, 34.77°E); 4S7B in Colombo, Sri Lanka (6.1°N, 80.22°E) and JA2IGY in Mt.

Asama, Japan (34.45°N, 136.78°E). The circuit path considered here is VR2B - ZS1HMO, which has a short path of 11 813 km and long path of 28 211 km.

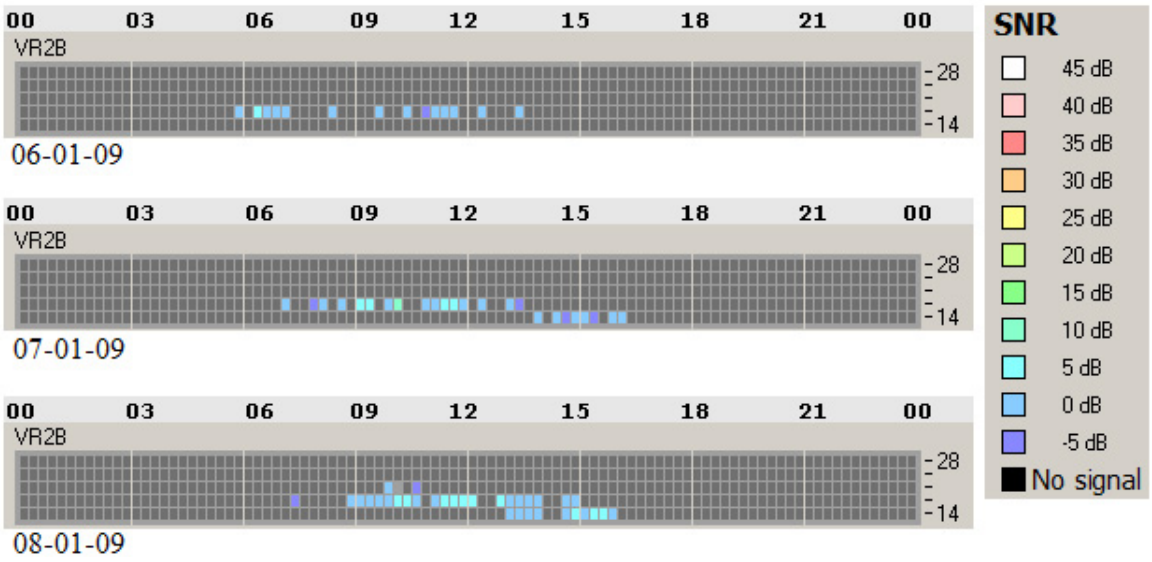

Figure 4.6: Reception of beacon signals from VR2B, Hong Kong.

Figure 4.6 shows that from 06-01-09 to 08-01-09, reception of beacon signals from VR2B occurs during local day time, 06h00 UT - 16h00 UT. The reception of the VR2B beacon signals is characterised by low SNR of less than 10 dB. Propagation is through 14.1 MHz and 18.11 MHz with very short weak openings on 21.15 MHz.

4.2.3 Europe

One beacon transmit from Europe: OH2B in Lohja, Finland (60.32°N, 24.83°E).

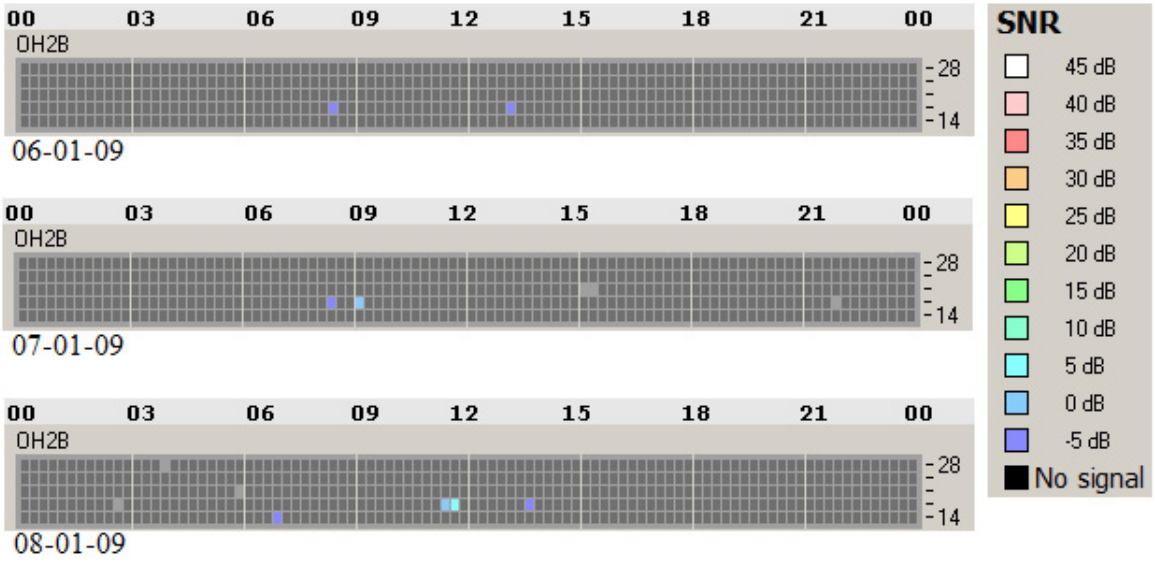

Figure 4.7: Reception of beacon signals from OH2B, Finland.

The circuit parth considered in Figure 4.7 is OH2B - ZS1HMO, which has a short path of 10 544 km and long path of 29 480 km. Figure 4.7 shows that there was very poor reception of beacon signals from OH2B. The signal quality was low, with SNR less than 15 dB. The signal reception occured in short openings throughout the day.

4.2.4 North America

Four beacons transmit from North America: VE8AT in Eureka, Nunavut, Canada (79.98°N, 85.95°W); 4U1UN in New York City, USA (40.75°N, 73.97°W); W6WX in Mt. Umunhum, USA (37.15°N, 121.90°W) and KH6WO in Laie, Hawaii (21.63°N, 157.92°W).The circuit parth considered here is 4U1UN - ZS1HMO, which has a short path of 12 653 km and long path of 27 370 km.

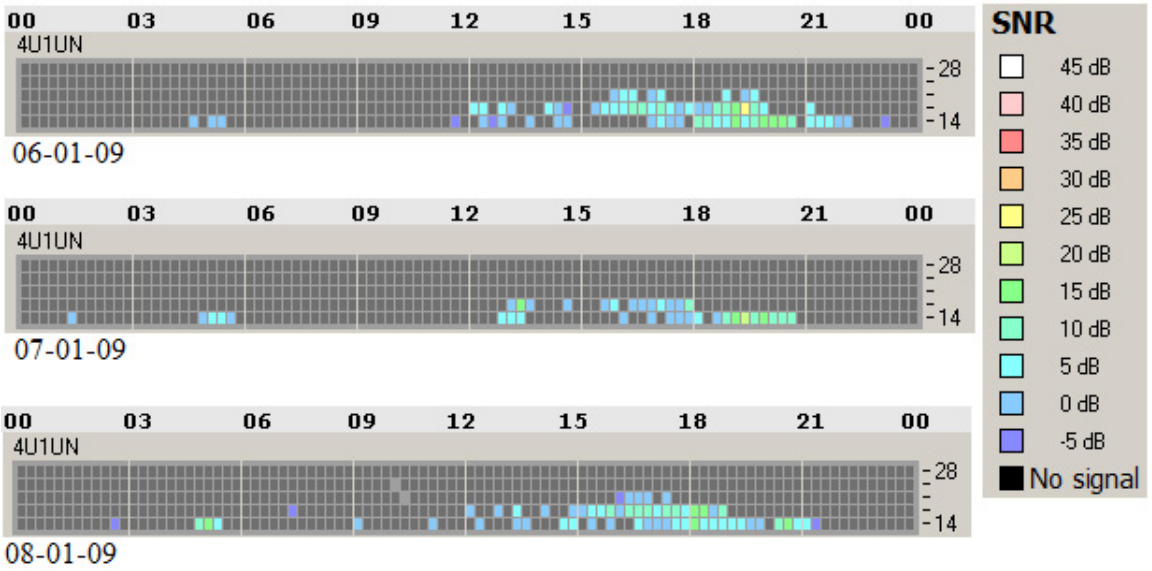

Figure 4.8: Reception of beacon signals from 4U1UN, New York.

Figure 4.8 shows that reception of beacon signals from 4U1UN generally occured through 14.10, 18.11 and 21.15 MHz on 6 - 8 January 2009. Brief band openings on 14.10 MHz are witnessed during the late local night hours, 05 UT to 06 UT, and wider openings on 14.10, 18.11 and 21.15 MHz during the late morning hours (15 - 21 UT).

4.2.5 South America

Three beacons transmit from South America: YV5B in Caracas, Venezuela (10.42°N, 66.85°W); OA4B in Lima, Peru (12.07°S, 76.95°W) and LU4AA in Buenos, Aires, Argentina (34.62°S, 58.35°W). The circuit path considered here is OA4B - ZS1HMO, which has a short path of 9 807 km and long path of 30 217 km.

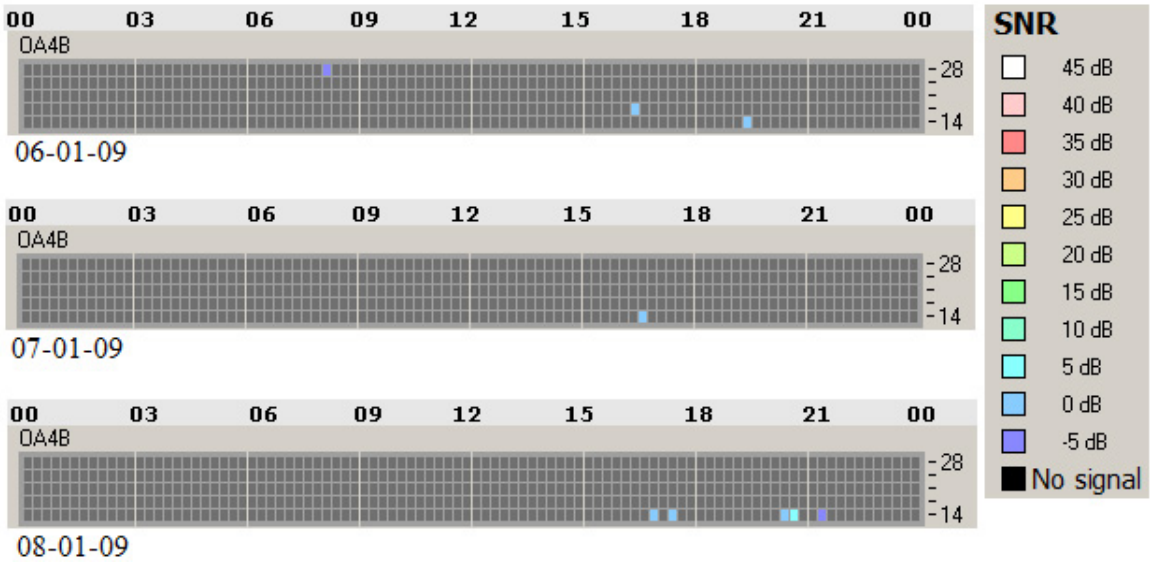

Figure 4.9: Reception of beacon signals from OA4B, Peru.

Figure 4.9 shows that reception of beacon signals from OA4B was very poor during 6 - 8 January 2009. Band openings on 14.10, 18.11 and 28.2 MHz were very short, with weak SNR of less than 5 dB.

4.2.6 Analysis of world wide beacon reception

The results generally show that, when radio communication takes place through skywave propagation, the received signal strength is not constant but varies with time, because of the fluctuations in ionospheric conditions. The reception of the IBP beacon signals is characterised by significant signal fading. Reception of signals from Africa are characterised by high SNR values and wide band openings whilst reception of signals from South America, North America, Asia and Europe is characterised by low SNR values and short band openings. This could be a result of high signal absorption over such long paths.

Davies (1969) points out that, with long distance propagation, the net propagation path can be a complicated summation of various hops, including different ionospheric layers. This may result in increased loss of energy during ground reflections between hops. Propagation between ZS1HMO and western locations, such as OA4B (Peru, South America) shows very weak SNR values and erratic band openings, as shown in Figure 4.9. This could be due to differences in ionospheric behaviour, which occurs when one part of the path is in darkness and the other in full sunlight. As a result, the signals may suffer excessive absorption. Simmons and Ace (1995) also stressed that, under certain conditions, the absorption of radio

frequency energy is so great that communication over any distance beyond line of sight becomes difficult.

Apart from the regular and irregular ionospheric variations, transmitter (Tx) and receiver (Rx) antenna heights, Tx and Rx antenna gain, Tx power and man-made noise at the Rx site also have a significant effect on beacon signal reception at the ZS1HMO monitor station. Hall (1995) indicated that a greater antenna height can be an advantage at certain times of the day for some paths and also that under certain conditions, when the LUF is just below a band, high antennas can widen the propagation window enough to allow radio communication that may be impossible with low antennas.

4.3 An application: Validation of ICEPAC model

Many amateurs and commercial radio communicators use HF propagation prediction software such as ICEPAC to determine HF band conditions and plan their communications. Beckwith *et al* (1974) pointed out that the applications of ionospheric prediction has been directed primarily towards the forecasting of ionospheric characteristics such as MUF and LUF for the design and operation of sky-wave telecommunication systems. The Southern African space weather website (http://www.spaceweather.co.za) uses ICEPAC to provide daily MUF, LUF, optimum working frequency (OWF) and take-off angle predictions for a range of bands in a bid to help users improve HF communication.

However, studies have indicated that real-time beacon data, when it is available, is useful for validations of such HF propagation predition models. Using the ICEPAC complete system performance (method 30), the predicted SNR values were compared with SNR measurements gathered by the ZS1HMO monitoring station. Results for the 5Z4B - ZS1HMO (Kenya to South Africa) and RR9O - ZS1HMO (Russia to South Africa) circuit paths are shown in sections 4.3.1 and 4.3.2, respectively. The measured and predicted SNR often decreased to levels below the noise level. Data points for SNR < 0 dB are not plotted.

4.3.1 5Z4B - ZS1HMO circuit path

For the 5Z4B - ZS1HMO circuit path, the measured and predicted transmissions were from Kariobangi, Kenya, 5Z4B (1.24°S, 36.88°E) and the receiving site was at Hermanus, South Africa, ZS1HMO (34.42°S, 19.22°E). The circuit is 4 119 km (SP) and 35 905 km (LP) in length. Figures 4.10 and 4.11 show the comparison between ICEPAC predictions and the real-time beacon measurements for selected

individual days during September 2008 on 14.1 MHz.

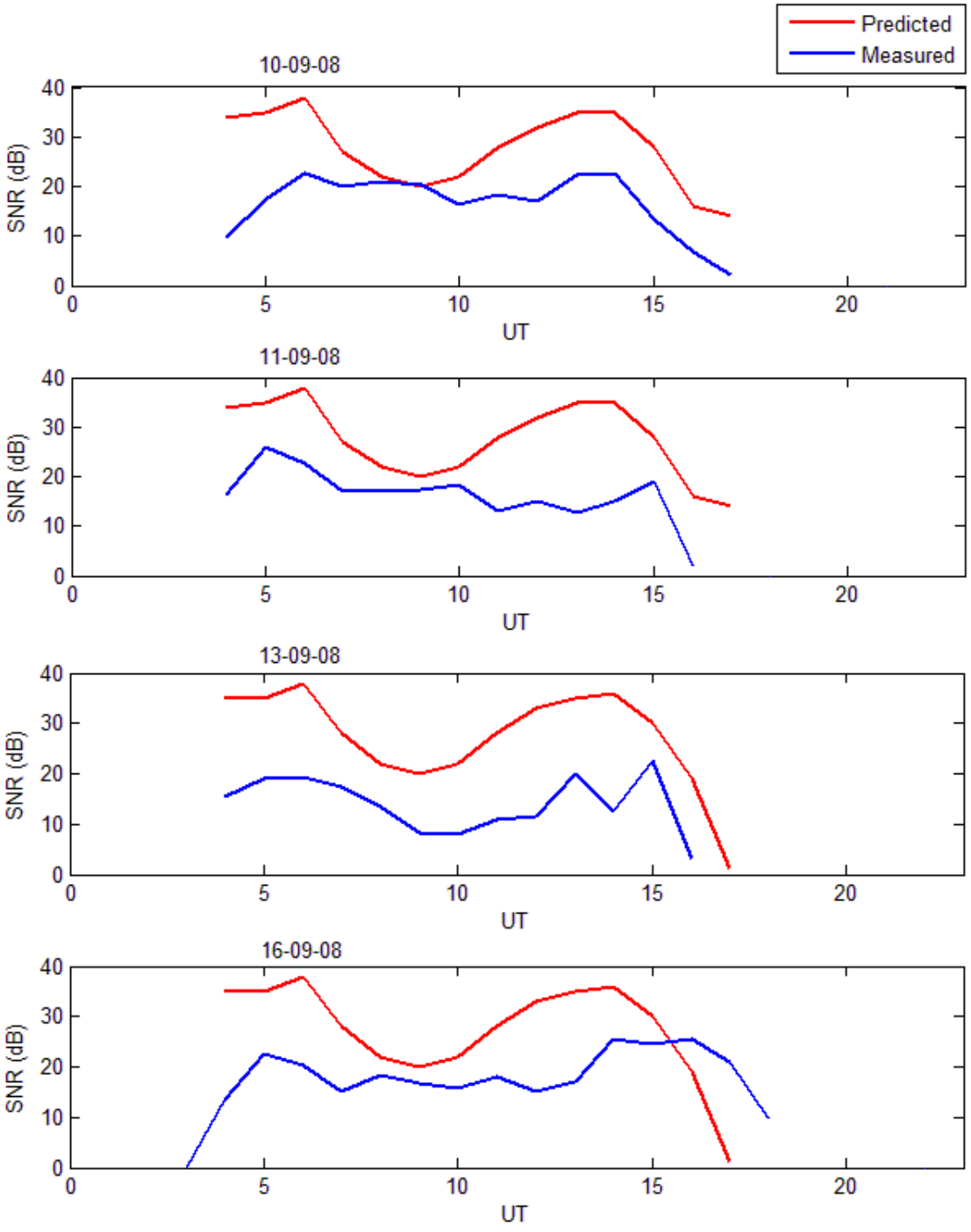

Figure 4.10: Comparison of predicted and measured SNR for 10, 11, 13 and 16 September 2008 on 14.1 MHz, for the 5Z4B - ZS1HMO path.

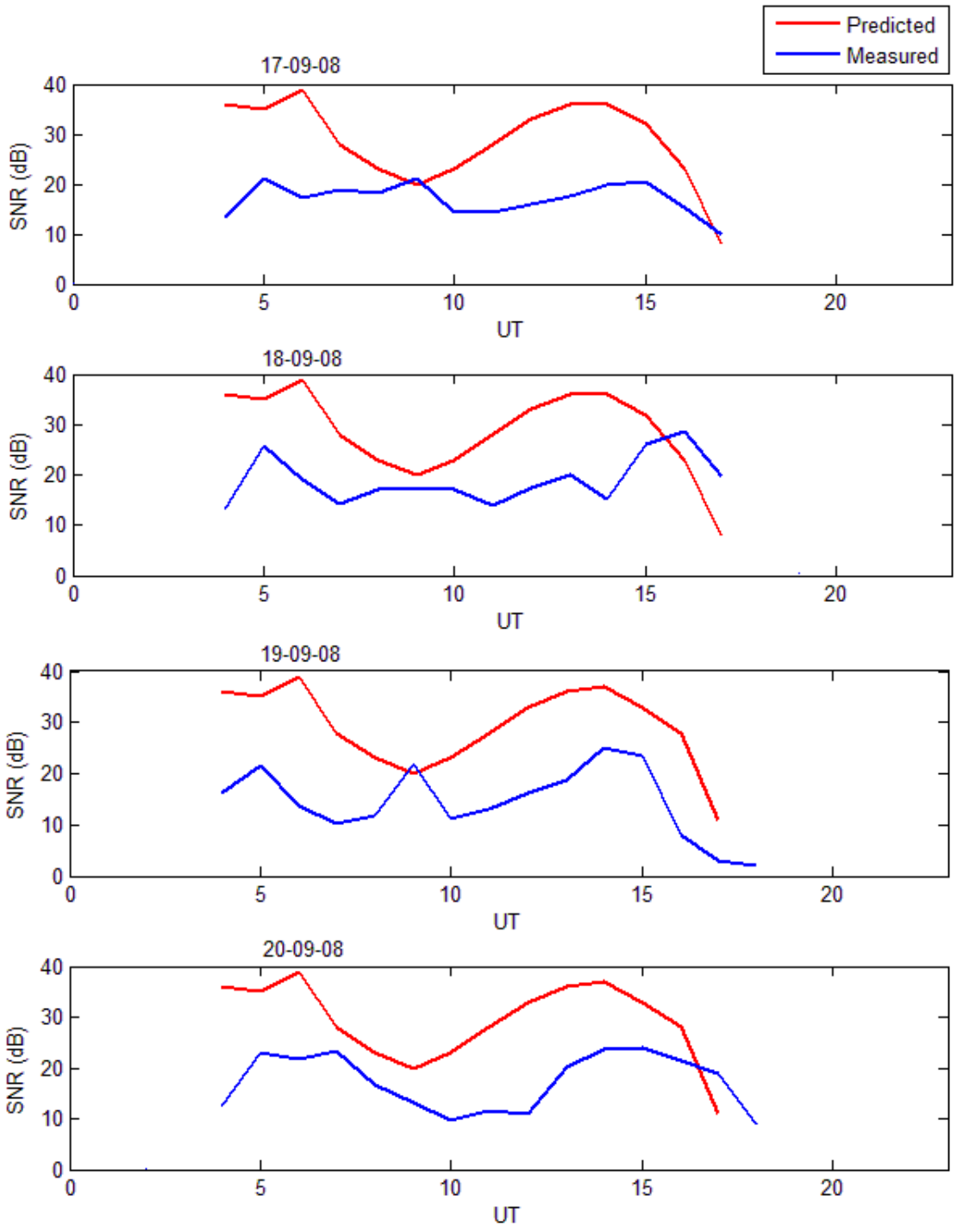

Figure 4.11: Comparison of predicted and measured SNR for 17, 18, 19 and 20 September 2008 on 14.1 MHz, for the 5Z4B - ZS1HMO path.

The plots in Figure 4.12 and Figure 4.13 show the comparison between ICEPAC predictions and the real-time beacon measurements for selected individual days in January 2009 on 14.1 MHz and Figures 4.15 and 4.16 show comparisons on 18.11 MHz.

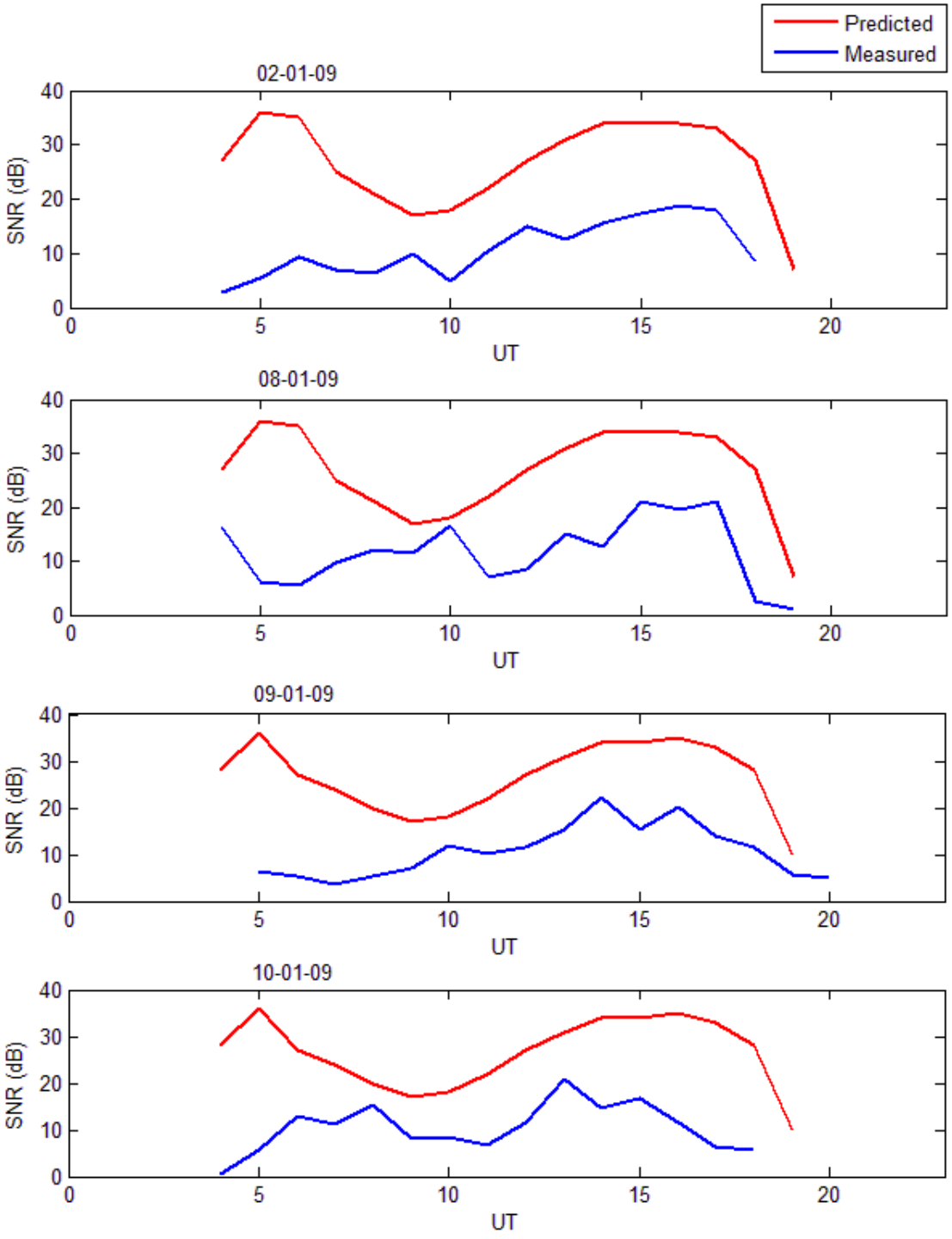

Figure 4.12: Comparison of predicted and measured SNR for 2, 8, 9 and 10 January 2009 on 14.1 MHz, for the 5Z4B - ZS1HMO path.

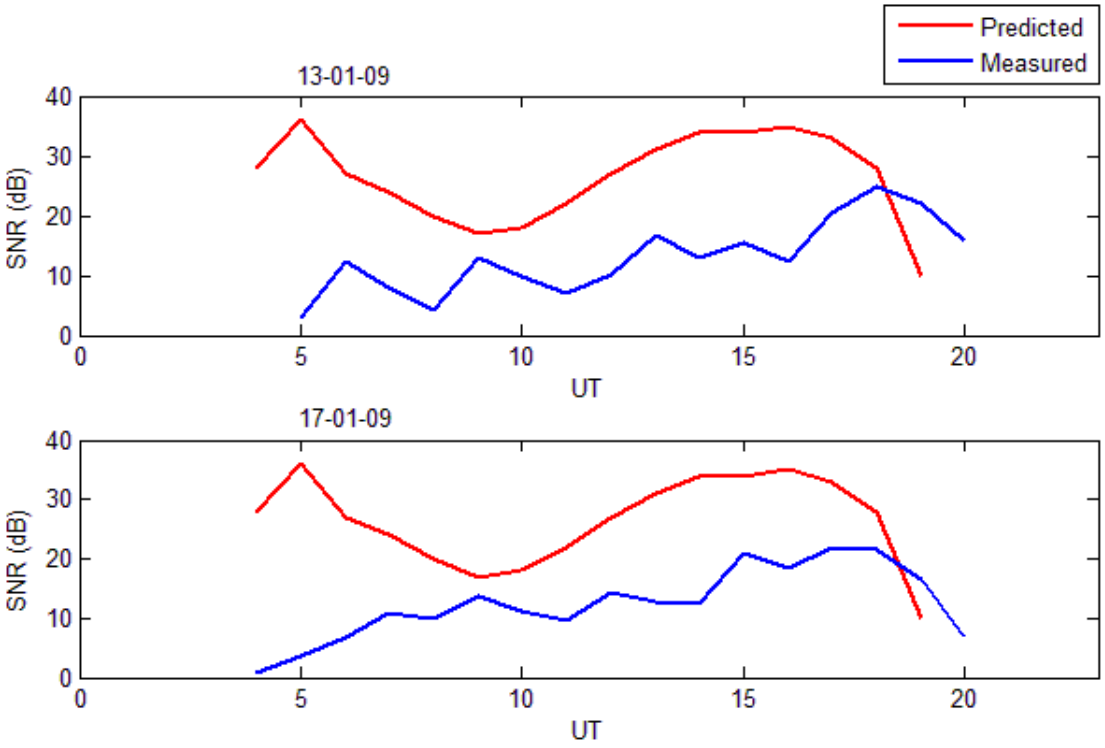

Figure 4.13: Comparison of predicted and measured SNR for 13 and 17 January 2009 on 14.1 MHz, for the 5Z4B - ZS1HMO path.

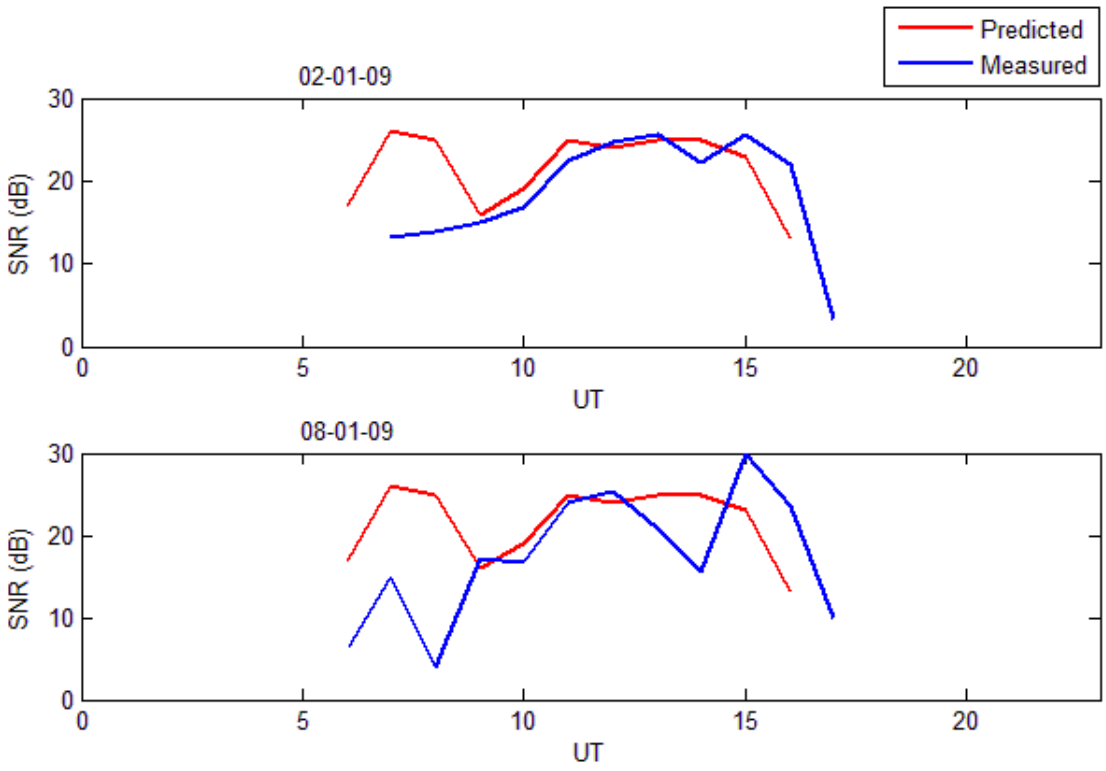

Figure 4.14: Comparison of predicted and measured SNR for 2 and 8 January 2009 on 18.11 MHz, for the 5Z4B - ZS1HMO path.

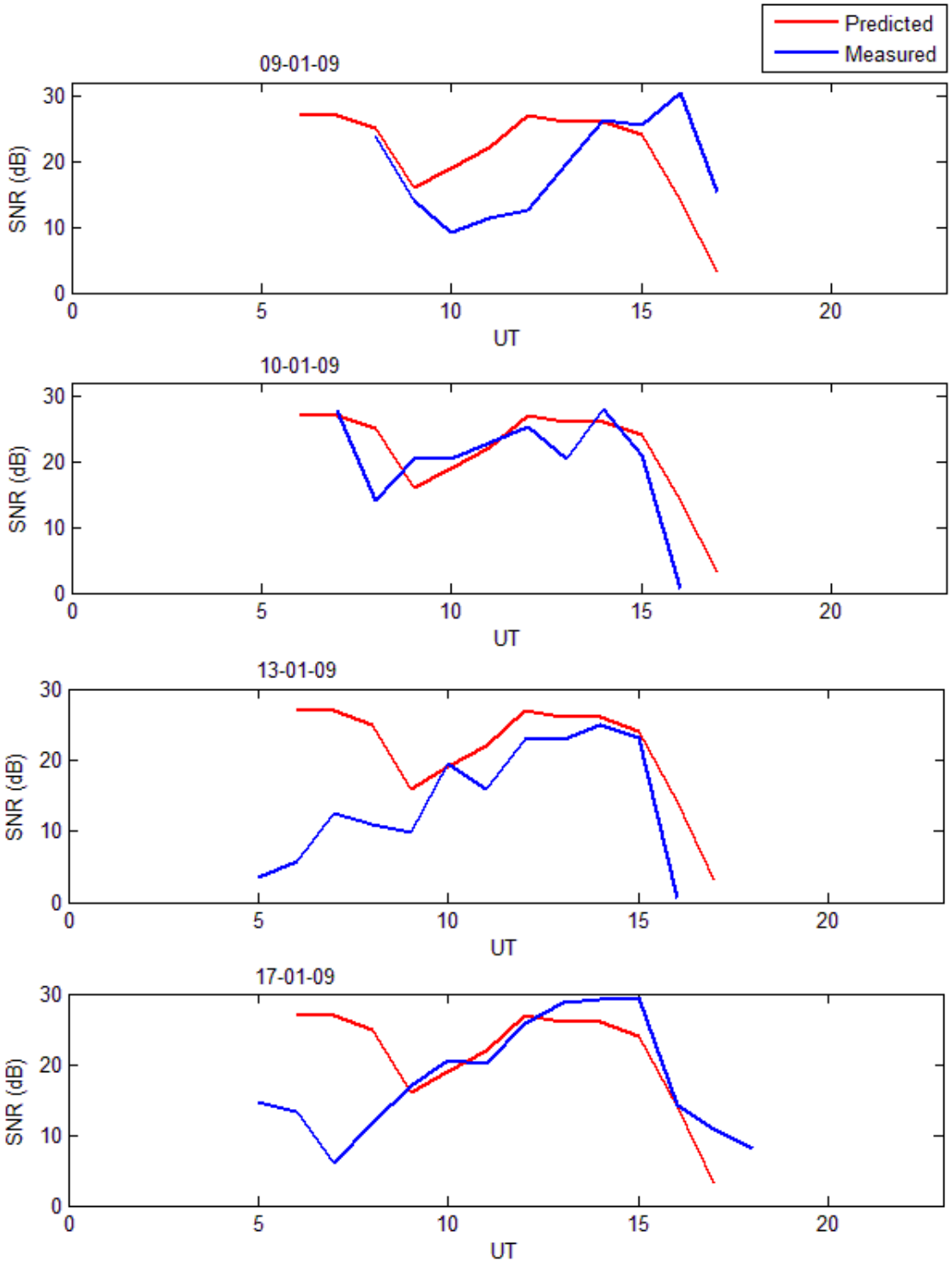

Figure 4.15: Comparison of predicted and measured SNR for 9, 10, 13 and 17 January 2009 on 18.11 MHz, for the 5Z4B - ZS1HMO path.

4.3.2 RR9O - ZS1HMO circuit path

For the RR9O - ZS1HMO circuit path, the measured and predicted transmissions were from Novosibirsk, Russia, RR9O (54.98°N, 82.90°E) and the receiving site

was at Hermanus, South Africa, ZS1HMO (34.42°S, 19.22°E). The circuit is 11 635 km (SP) and 28 388 km (LP) in length. Figures 4.16 and 4.17 show the comparison between ICEPAC predictions and the real-time beacon measurements for selected individual days in September 2008 on 14.1 MHz.

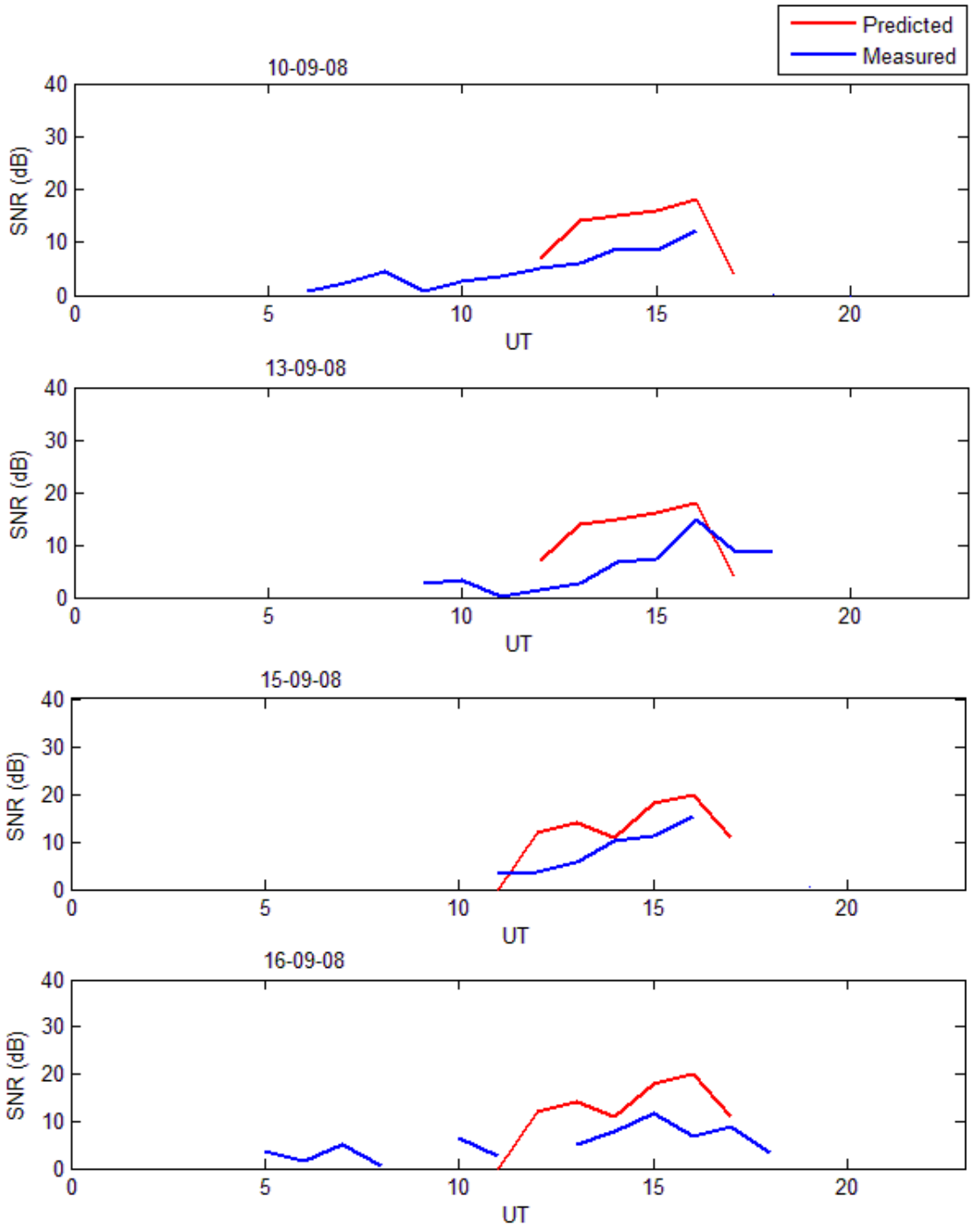

Figure 4.16: Comparison of predicted and measured SNR for 10, 13, 15 and 16 September 2008 on 14.1 MHz, for the RR9O - ZS1HMO path.

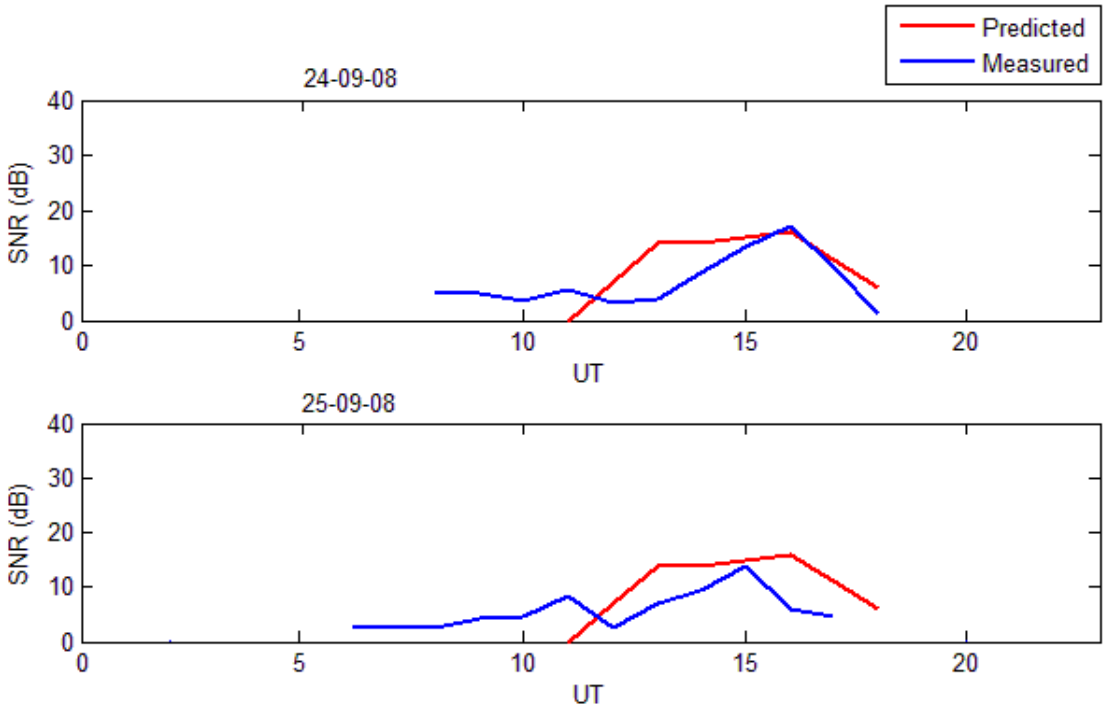

Figure 4.17: Comparison of predicted and measured SNR for 24 and 25 September 2008 on 14.1 MHz, for the RR9O - ZS1HMO path.

4.3.3 Analysis of the results of validating ICEPAC

Comparison between ICEPAC predictions and beacon measurements show that the SNR has a diurnal dependence and a variability that is probably due to the changing ionospheric conditions. Figures 4.10 - 4.17 compare the circuit path SNR measurements and predictions, clearly illustrating the differences in signal variation. From these figures it can be noted that the predicted SNR curves do not exactly match the measured SNR curves, which is attributed to a poor ICEPAC prediction of circuit perfomance.

Comparisons on 14.1 MHz (Figures 4.10, 4.11, 4.12 and 4.13) are characterised by large differences between predicted and measured SNR values. The plots show that ICEPAC predicts higher SNR values compared to the measurements. This may be due to the possibilty that ICEPAC underestimates circuit path loss. As a measure of ICEPAC's prediction ability, the root mean square deviation ($RMSD$) was calculated per day as follows:

$$RMSD = \sqrt{{}^{1}/_{N} \sum_{i=1}^{N} (SNR_{meas} - SNR_{pred})^2} \tag{4.1}$$

where N is the number of data points which is equivalent to the number of hours

in a day, SNR_{meas} is the SNR measured by the ZS1HMO monitoring station and SNR_{pred} is the SNR predicted by the ICEPAC model.

Table 4.1 shows the RMSD for the 5Z4B - ZS1HMO and RR9O - ZS1HMO paths.

(A)

Day	*RMSD (dB)*
10	41.6
11	47.5
13	55.2
16	34.1
17	43.3
18	37.6

(B)

Day	*RMSD (dB)*
10	15.3
13	13.0
15	10.5
16	11.5
24	9.4
25	10.2

Table 4.1: RMSD computed per day for selected days in September 2008 for (A) the 5Z4B - ZS1HMO path and (B) the RR9O - ZS1HMO path.

Table 4.1 clearly shows that the circuit 5Z4B - ZS1HMO provides a higher RMSD than the RR9O - ZS1HMO circuit, also implying that the 5Z4B - ZS1HMO path has higher residual errors ($SNR_{meas} - SNR_{pred}$) than the RR9O - ZS1HMO path. This shows that ICEPAC prediction accuracy is higher on transmission from RR9O (Europe) as compared to transmissions within Africa (5Z4B). It is also interesting to note that ICEPAC's prediction ability depends on the frequency, as shown in Table 4.2. For the 5Z4B - ZS1HMO path, 14.1 MHz show higher RMSD as compared to 18.11 MHz.

Day	*RMSD (dB)*	*RMSD (dB)*
	14.1 MHz	*18.1 MHz*
02	67.1	6.2
08	59.5	12.6
09	59.5	10.1
10	66.6	8.4
13	52.6	25.3
17	56.8	6.4

Table 4.2: RMSD computed per day for selected days in January 2009 for the 5Z4B - ZS1HMO path on 14.1 MHz and 18.11 MHz.

The deviation of the predicted SNR from the measured SNR might possibly be due to predictions being based upon median data, therefore resulting in median output parameters, as also mentioned by De Canck (2006b). De Canck(2006b) also points out that the ionospheric conditions are changing constantly and probably deviating from the median conditions. In addition, the ionospheric behaviour model in ICEPAC is hardwired into the software and it is apparently not possible to make any adjustments to the ionosphere based on local knowledge.

However, by inspection, Figures 4.10 - 4.17 show that the predicted SNR follows more or less the same daily trend every month whereas the measured SNR show considerable variation every day of the month. In Figures 4.18 and 4.19, the error bars show the standard deviation of the dispersion of the predicted and measured SNR values from their monthly average, in terms of standard deviation, for 14.1 MHz on 17 September 2008. The predicted SNR shows very little deviation from the monthly average SNR values, except for the circled hours. In Figure 4.19, the measured SNR generally shows large deviations from the monthly mean.

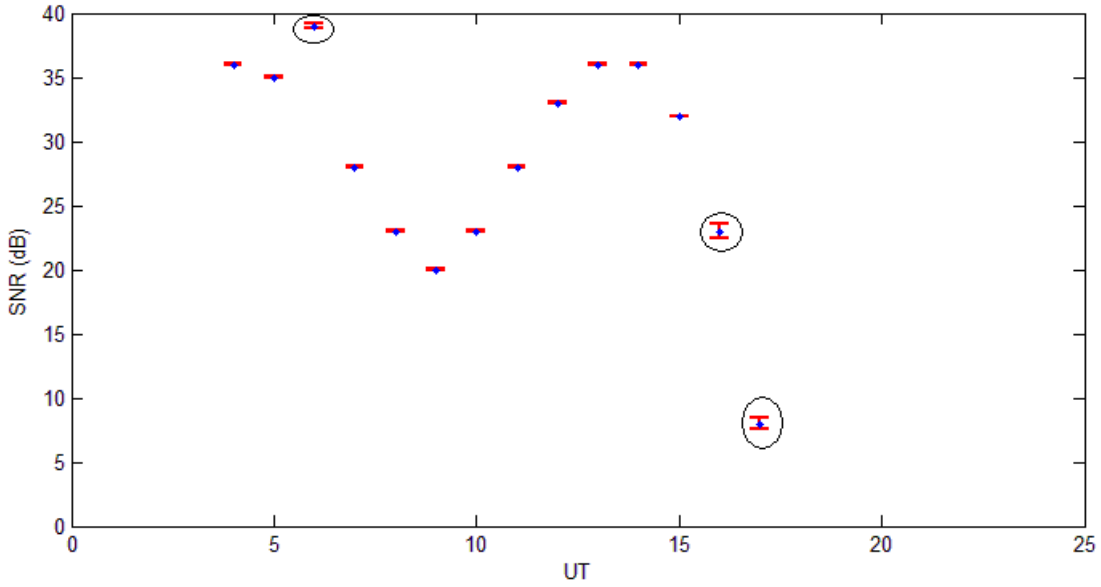

Figure 4.18: Error bars showing the amount of deviation of the predicted SNR from the monthly mean for each UT hour on 17 September 2008 for 14.1 MHz.

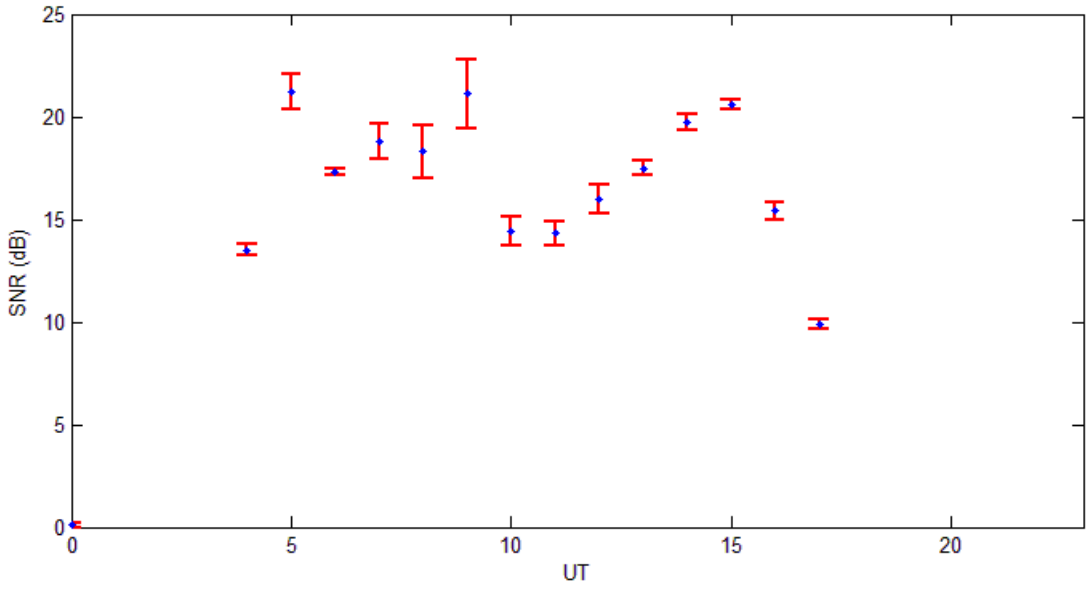

Figure 4.19: Error bars showing the amount of deviation of the measured SNR from the monthly mean for each UT hour on 17 September 2008 for 14.1 MHz.

Chapter 5

Conclusion

The aim of the study presented in this thesis was to set up an automated monitoring/receiving station for international HF beacons at the Hermanus Magnetic Observatory (HMO) based in Hermanus, South Africa. The worldwide network of beacons monitored in this study is maintained and operated by the NCDXF/IARU International Beacon Project and they transmit on five HF frequencies, namely: 14.1, 18.11, 21.15, 24.93 and 28.2 MHz.

There are regular and irregular variations that affect ionospheric radio propagation, as discussed in chapter 2 of this thesis. Taking variability and other factors into account, the only reliable way to know what the prevailing ionospheric HF radio propagation conditions are, is to listen to the IBP beacons. In this study, the most convenient and effective way of listening to the beacons was through the ZS1HMO automatic monitoring station, the set-up of which is discussed in chapter 3 of this thesis. Successful upgrading of the single band to multiband monitoring station involved a number a key factors, such as the installation of the multiband antenna, the construction and installation of the CI-V level converter; and the provision of fast internet connection to the HMO time server for Faros software to obtain an accurate time reference and maintain its own software clock. These factors, among others, maintained the correct and reliable operation of Faros in logging the beacon observations in real time.

Chapter 3 of this thesis clearly shows that the NCDXF/IARU International Beacon Project is indeed a useful tool in studying real-time HF propagation conditions. Much can be learnt from monitoring the IBP beacons on the five HF bands. The discussion in section 4.1 confirms that the real-time signal plots (Figures 4.1, 4.2, 4.3 and 4.4) can be shared with other HF radio users, such as amateur radio operators and military users, through the internet as an indicator of prevailing HF propagation conditions on the 14 - 28 MHz bands. The real-time signal plots, as well as the archive of historical signal plots available on the ZS1HMO monitor-

ing webpage (http://spaceweather.hmo.ac.za) convey information on propagation conditions to users in terms that are easy to interpret and understand.

Section 4.3 of this thesis demonstrates that the ZS1HMO beacon measurements can also be used to validate HF propagation models, thereby providing information on how they perfom over Africa and other parts of the world. ICEPAC is an HF propagation prediction model that is being used to provide predictions for the Southern African Space Weather website. Figures 4.14 to 4.17 shows the inability of ICEPAC, for the given location and frequency, to match real time beacon measurements.

5.1 Possible future work

Considerations for improvements on this work in the future include:

- Construction of another multiband antenna that is designed to resonate specifically on the IBP bands i.e 20, 17, 15, 12 and 10 m. The G5RV multiband antenna used in this study was originally designed to operate as a 3/2 wavelength center-fed antenna for 14 MHz (Varney, 1985), and resonates only on two bands (20 and 12 m). The ZS6BKW multiband antenna can be a possible choice, since it resonates on five bands, including, 20, 17and 10 m.

- Since all the IBP transmitters use vertical monopole antennas, it would be ideal to install a vertical monopole antenna at ZS1HMO to monitor the beacons and possibly compare its performance to other multiband antennas, such as the MFJ-1778 G5RV that is currently being used.

- The "delay" parameter, that is measured by the ZS1HMO monitor station, can be used to study ionospheric propagation delay. To make accurate use of this parameter, in addition to the HMO time server used in this study, more time servers should be connected to the Faros monitoring software by means of the internet, so that the Faros can maintain a very accurate clock and hence measure the delays accurately.

- Installation of at least one beacon in each province of South Africa for the South African Radio League (SARL)/HMO 40 m beacon project. The SARL/HMO beacon project is a national system of beacons on the 40 metre band, operating on 7.023 MHz. Having the beacons in all provinces can provide a convenient network for detecting HF propagation conditions. Figure

5.1 shows the possible locations of such beacons in all provinces in South Africa.

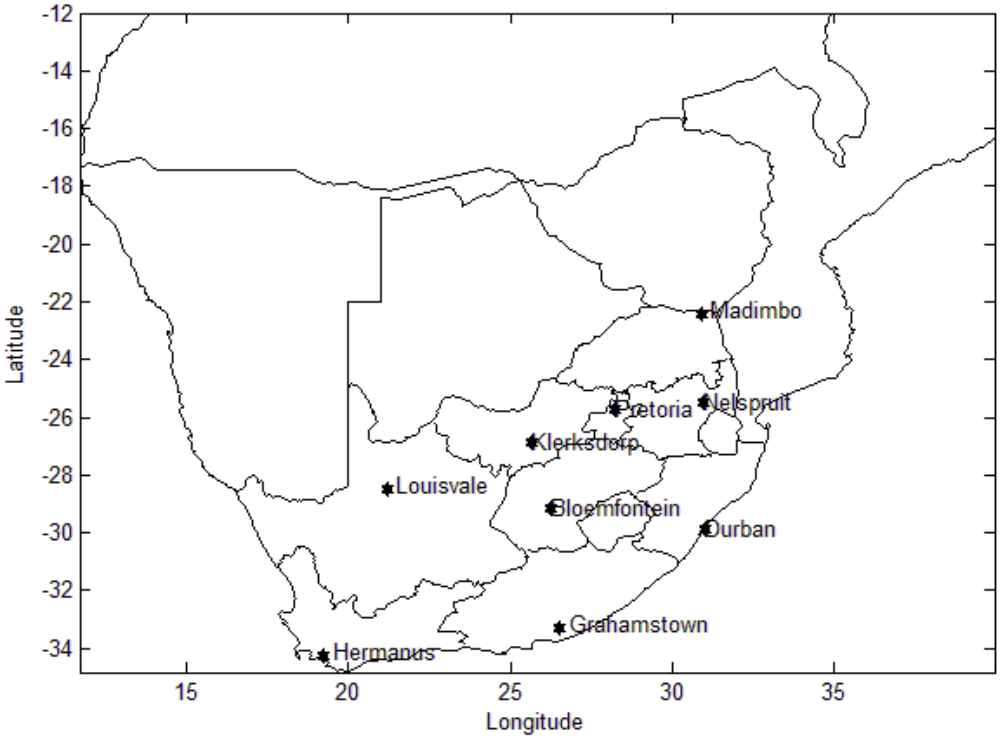

Figure 5.1: Map of South Africa showing the possible locations for 40 m beacons in all the provinces.

To summarise, the work presented in this thesis shows the interesting characteristics of HF radio wave propagation and its dependence on the behaviour of the ionosphere. For the Southern African region it is possible to improve substantially on HF propagation predictions and to provide a more efficient prediction service, with higher levels of accuracy and a more reliable map of ionospheric behaviour.

References

Andress K, K7NV, Cebik L.B, W4RNL, Severns R, N6LF, Lewallen R, W7EL and Frank W, AI1H, "The ARRL Antenna Book, 19th Edition", ARRL, the National Association for Amateur Radio, Newington, CT, USA, 2000.

Banks P.M and Kockarts G, "Aeronomy Part A", Academic Press, New York, 1973.

Beckwith R.I, Bailey A.D and Narayana N.R, "Application of ionospheric predictions to HF propagation in three dimensions", Radio Science, Vol 9, 379-385, 1974.

Brasseur P.G and Solomon S, "Aeronomy of the middle atmosphere: chemistry and physics of the stratosphere and mesosphere: Third revised and enlarged edition", Springer, Netherlands, 533, 2005.

Carr J.J, "Practical Antenna Handbook, Fourth Edition", McGraw-Hill Professional, New York, 2001(a).

Carr J.J, "Antenna Toolkit, 2nd Edition", Newnes, Oxford, 2001(b).

Davies K, "Ionospheric radio waves", Blaisdell, Watham, MA, USA, 1969.

De Canck M.H, ON5AU, "Do we need to learn about propagation?" antenneX, Issue No. 115, November 2006(a).

De Canck M.H, ON5AU, "Propagation prediction programs explained-Part 20", antenneX, Issue No. 109, May 2006(b).

Dennison M, G3XDV, Lorek C, G4HCL, "Radio Communication Handbook, 8th Edition" Radio Society of Great Britain, Hertfordshire, England, 12.19, 2005

Hall J, KT1TD, "Interpreting QST's new propagation charts for low power and low antennas" QST, 3, 1995

Icom, " ICOM Instruction manual, HF Transceiver IC-728, HF/50 MHz Transceiver IC-729", ICOM Incorporated, Hinaraka, Osaka, Japan, 1992.

ICOM, "Icom CT-17 Intsruction manual", ICOM Incorporated, Hinaraka, Osaka, Japan, 1986.

ITS, "Ionospheric Communications Enhanced Profile Analysis & Circuit (ICEPAC) prediction program users manual", Institute for Telecommunication Sciences, Boulder, Colorado, 2007.

Lane G., "Review of High Frequency Ionospheric Communications Enhanced Profile Analysis & Circuit (ICEPAC) prediction program", Ionospheric Effects Symposium, Alexandria, VA, May 3-5, 261-1 - 261-8, 2005.

Laster C, W5ZPV, "The beginner's handbook of amateur radio, 3rd edition", McGraw-Hill Professional, Blue Ridge Summit, 2000.

Lusis J. D, "HF Propagation: The basics", QST, 1983.

Maslin N.M, "HF communications: A system approach", CRC Press, USA, 1987.

McNamara L.F, "The Ionosphere: Communications, Surveillance, and Direction Finding", Krieger Publishing Company, Malabar, USA, 1991.

McNamara L.F, Bullet T.W, Mishin E, and Yampolski Y.M, "Nighttime above-the-MUF HF propagation on a midlatitude circuit", Radio Science Vol. 43, 10.1029/2007RS003742, March 2008.

Milligan T.A, "Modern Antenna Design", John Wiley and Sons, Hoboken, NJ, USA, 4, 2005.

NCDXF Online: http://www.ncdxf.org/Beacon/intro-html/, accessed 2009.

Orr W.I and Cowan S.D, "Beam Antenna Handbook", Watson-Guptill Publications Inc, 1990.

Rhodes J.E, "Antenna Handbook, MCRP 6-22D", U.S. Marine Corps, 1999.

Seybold J.S, "Introduction to RF Propagation", John Wiley and Sons, Hoboken, NJ, USA, 2005.

Simmons L.D and Ace F.L III, "Electronics Technician Volume 7 - Antennas and Wave Propagation", Naval Education and Training (NAVEDTRA 14 092), Proffesional Development and Technology Centre, U.S Navy, 1995.

Sizun H, "Radio wave propagation for Tellecommunication Applications", Springer-Verlag Heidelberg, 2005.

Teters L.R., Lloyd J.L., Haydon G.W. and Lucas D.L, " Estimating the perfomance of telecommunication systems using the ionospheric channel: (Volume II) Ionospheric Communications Analysis and Prediction Program user's manual", Institute for Telecommunication Sciences NTIA Report 83-127, July 1983.

Troster J.G., W6ISQ and Fabry R.S., N6EK, "The NCDXF/IARU International Beacon Project. Report and update", QST, pp47-47, Sptember 1997.

Varney L, G5RV, "The G5RV multiband antenna: Up-to-date", The ARRL Antenna Compendium Vol. 1, 86-90, 1985.